

Revision of the paper: “Aethalometer multiple scattering correction C_{ref} for mineral dust aerosols” by C. Di Biagio et al.

Answers to reviewers

The authors wish to thank the reviewers for their valuable comments which helped to improve the quality and readability of the manuscript. Answers to the reviewer’s comments are reported in the following (questions in black, **answers in red**).

Referee #1

The authors have done a commendable job of executing a well-designed experiment to measure C_{ref} for mineral dust aerosols. The experimental methods were carefully designed, with sufficient redundancy to test closure in the data. They applied the measurements to several aerosol types to determine the role of single scatter albedo and wavelength dependence on their values. The manuscript is well written and I recommend the paper be published after attending to minor comments below.

Line 12: I suggest spelling out “CAPS PMex”, and including “respectively” after “nephelometer”.

The text was changed accordingly.

Line 19: Change “The calculated mean C_{ref} ..” to “The calculated mean and one standard deviation C_{ref} ”, or something along those lines so the reader knows what the numbers in parentheses refer to.

The text was changed accordingly.

Line 21: Does the $C_{ref}=2.14$ correspond to a specific wavelength? If so, include here.

This has been rewritten as: “..higher than that obtained by using $C_{ref}=2.14$ at both 450 and 660 nm, as usually assumed in the literature”.

Line 22: Does the 3% change correspond to both wavelengths?

The change corresponds to the 660 nm wavelength. This is now specified in the abstract.

Line 26: Include “respectively” after 660 nm.

The text was changed accordingly.

Line 52: Include “such” between “species” and “as soot”

The text was changed accordingly.

Line 54: The “-“ in my version reads as a division sign, between ~100-100000 and ~0.1-100.

The text was changed accordingly.

Line 99: Can the authors clarify as to what they mean by “optimized”?

The sentence was rewritten as: “Henceforth, in this work we present the experimental estimate of C_{ref} for mineral dust aerosols at 450 and 660 nm obtained from a laboratory-based intercomparison study.”

Line 109: Correct “wavelentgh” to “wavelength”

The text was changed accordingly.

Line 121: Same as previous comment.

The text was changed accordingly.

Line 137: Please clarify sentence “so the same aerosol size distribution as input for all instruments”. It seems to be missing a word.

The sentence was rewritten as: “Their length, varying between 0.3 and 0.7 m, was adjusted based on the flowrate of each instrument to ensure an equivalent particle loss, so that the same aerosol size distribution is in input to the different instruments.”

Line 189: Should $\ln(\text{ATN})$ in equations 6a and 6b be $\ln(\text{ATT})$?

The text was changed accordingly.

Line 276: Can the authors provide more detail regarding how this “conversion” was accomplished? Did they calibrate the OPC to provide a parameterization between refractive index and geometric and optical size? Can they comment on the role of relative humidity and how this might impact their data, since it didn’t appear, especially in the ambient outdoor measurements, that they controlled RH? Addition of water would affect refractive index and change the instrument response.

This part was rewritten as: “The OPC optical-equivalent nominal diameters were converted into sphere-equivalent geometrical diameters (D_g) by taking into account the aerosol complex refractive index. This consisted in recalculating the OPC calibration curve for different complex refractive index values. For dust aerosols the refractive index was varied in the range 1.47-1.53 (n) and 0.001-0.005 i (k) following the literature (see Di Biagio et al., 2017) and D_g was set at the mean \pm one standard deviation of the values obtained for the different n and k . For kaolinite the OPC diameter conversion was performed by setting the refractive index at 1.56-0.001 i . For ambient air the refractive index was set at 1.60-0.01 i , a value that represents a medium absorbing urban polluted aerosol (see Di Biagio et al., 2016). The impact of humidity on the refractive index of ambient aerosols and associated changes OPC response are not taken into account. The relative humidity was always below 35% during ambient air measurements, which implies a very small particle growth.”

Line 270: Please state the size range of the fine and coarse mode. It can be read off the integrals in equations 12 and 13 but would be clearer in the text.

The size ranges of the fine and coarse modes are now explicitly stated in the main text.

Line 299: Were all of the Niger samples from size different areas combined to form 2 for the experiments?

The two Niger samples, as reported in Table 2, correspond to the same soil sample collected at the rural area of Banizoumbou. We decided to duplicate the experiments for the Niger soil in order to test the repeatability of the results.

Line 314: Why was the OPC not included in this control? (line 309-310).

The main objective of the control experiment was to verify the performance of optical instruments. We did not consider in this case necessary to have a redundancy also on size distribution data.

Line 342: Change “251” to “2.51” (I assume this is a typo).

The text was changed accordingly.

Line 380: Can the authors mention what the error bars refer to in this Figure and in the discussion for the following figures?

The captions of Fig. 5, 6, and 8 have been modified to include an explanation of what error bars refer to.

Line 465: What about the dependence of C_{ref} and the coarse component at 450nm? (Figure 8, lower left).

The dependence found for C_{ref} at 450 nm against $D_{eff,coarse}$ can be related to the fact that when large absorbing ambient aerosols deposit on the filter the scattering from the filter fibres can increase due to some multiple scattering with these particles. However, this is just a hypothesis and a more detailed investigation on this topic should be addressed to clarify this behaviour. Given that the main focus of the paper is on mineral dust we decided not to comment this result in the paper.

Referee #2

This is a very nice paper – it’s well-written and describes a well-designed experiment with useful results. The paper is appropriate for AMT. Kudos to the authors for making multiple checks/closure investigations on the measurements to make sure the data were consistent. I’ve made some minor editorial suggestions below. I guess some might also be considered science comments, but they are also minor.

Minor editorial and minor science comments:

Line 40 – Replace ‘As for today,’ with ‘Currently’

The text was changed accordingly.

Line 52 – Change to ‘This is particularly true when compared to other aerosol species, such as soot, for which...’

The text was changed accordingly.

Line 57 – should be ‘...global scales...’

The text was changed accordingly.

Line 69-70 – Change to ‘One instrument used to obtain aerosol light absorption...’

The text was changed accordingly.

Line 72-73 – Change to ‘The aethalometer reports equivalent black carbon mass Concentration ...’ [comment: Petzold et al 2013 suggest the terminology ‘equivalent black carbon’]

The text was changed accordingly.

Line 98 – Change to ‘Thus, the value of...’

The text was changed accordingly.

Line 119 – Change to ‘The MAAP is commonly assumed to provide the most reliable filter-based, direct estimate...’ [I think photoacoustic spectrometers are typically considered more reliable than filter based absorption measurements as there’s no filter involved to confound the measurement]

The text was changed accordingly.

Line 122 – Change to ‘...although Müller et al. (2011) measured...’

The text was changed accordingly.

Line 123 – wavelength is spelled wrong

The text was changed accordingly.

Line 134 – Move to Line 108 after the sentence ‘The experimental set-up...’ and change so it reads ‘Instrumental details and uncertainties are summarized in Table 1.

The text was changed accordingly.

Line 156-159 – say whether any conditioning (drying) was done to ambient particles.

The sentence was changed in: “-ambient pollution aerosols were sampled by opening the manifold to the exterior ambient air. Ambient aerosols were not dried.”

Line 258 – change to ‘...which was then applied to extrapolate beta_sca to 630 and 660 nm.’

The text was changed accordingly.

Line 285 – missing parenthesis around ‘13’ [comment – I’d probably call these equations 12a and 12b or just have one equation with d1 and d2 and say the range is 0.3-1.0 um for fine and 1-10 um for coarse.

The text was changed accordingly.

Line 295++ – change to ‘...uncertainties of...’ [Comment – I think it’s more common/standard to refer to the ‘uncertainty of’ rather than the ‘uncertainty on’ so lots of instances to change in this paragraph

The text was changed accordingly.

Line 317 – change to ‘...performance of the...’

The text was changed accordingly.

Line 320 – change to ‘This is further demonstrated by...’

The text was changed accordingly.

Line 316-324 –instrument uncertainties are listed in Table 1. This would be a good place to cite the instrument uncertainties and note that the difference is well within the uncertainties for the two instruments. Sherman et al (2015) supplemental materials is a good reference for the nephelometer uncertainties.

Part of the paragraph has been rewritten as: “As expected for this purely scattering aerosol (Toon et al., 1976), the nephelometer scattering and the CAPS extinction at 450 and 630 nm were in very good agreement (less than 4% difference) during the whole duration of the

experiment. This is well below the single instrument uncertainty of $\pm 9\%$ for the nephelometer (Sherman et al., 2015) and $\pm 5\%$ for the CAPS (Massoli et al., 2010)."

Line 351 – change to 'In contrast, for more absorbing...'

The text was changed accordingly.

Line 361-362 – Probably should move this sentence into previous sentence rather than have a 1 sentence paragraph. In some ways it seems in conflict with the previous paragraph where you discuss C_{ref}s being larger/smaller than each other depending on the ATT threshold. Can you make a plot or include numbers for the lower threshold in a table to definitively demonstrate that the 10 or 20% ATT threshold doesn't make a difference? Or maybe just put this sentence (lines 361-362) in the previous paragraph before the larger/smaller discussion so that the reader knows that, despite the C_{ref}s being larger or smaller for the 10% versus the 20% threshold, the absolute difference is very small.

The paragraph has been rewritten as: "Differences within 2.8% were obtained between C_{ref}^{*}, C_{ref}(W2003) and C_{ref}(C2010) at 450 and 660 nm for weakly-absorbing dust and kaolinite. In contrast, for more absorbing ambient air aerosols the differences between C_{ref}^{*}, C_{ref}(W2003) and C_{ref}(C2010) were in the range 2.7% to 24.3%. The different ATT threshold assumed here (20%) compared to W2003 and C2010 (10%) has a negligible impact (less than 1% difference) on the results. In some cases (ambient air 1–2 and Niger 1 samples), however, we obtained C_{ref}(C2010) > C_{ref}(W2003); these cases correspond to a mean aethalometer measured ATT < 10%, for which R(W2003) > R(C2010), and this explains the larger C_{ref}(C2010). Conversely, C_{ref}(C2010) < C_{ref}(W2003) when the measured ATT was ~15-20%, yielding R(W2003) < R(C2010). The percent difference between the obtained C_{ref}(W2003) and C_{ref}(C2010) increased for decreasing SSA due to the increase of the R(W2003) to R(C2010) absolute difference for decreasing SSA. When averaging data for all ambient air samples, the two formulations yield very similar values. For example, at 660 nm the mean C_{ref}(W2003) was 2.44 (± 0.38), less than 2% larger than the mean C_{ref}(C2010) of 2.39 (± 0.35)."

Line 364 - change to '...are reported...'

The text was changed accordingly.

Line 372-381 - Were the ambient aerosol particles dried in any way? If not, does the ambient SSA vary with ambient and/or measurement RH? (I don't know, but am guessing Paris might be damp/humid in November). The TSI nephelometer tends to run warmer than many other instruments so potentially could have discrepancies in scattering estimate if neph measure of scattering drives off more water than CAPS-MAAP estimate of scattering. There's a slight suggestion of that in Fig 4 where I think the lowest group of extinction points are for ambient air and they look to be more below the 1:1 line than the other points (fig 4 is log scale, so hard to tell!). The closure still looks great and the focus of this paper was on lab generated dust so I'm more just curious.

Ambient air is not dried (this is now explicitly stated in the main text). The nephelometer RH during ambient air measurements was between 20-35%, against the <15% RH during kaolinite, dust, and ammonium sulfate experiments. As discussed by the reviewer, the possible difference in RH conditions between the three optical instruments (nephelometer expected to have larger RH compared to the CAPS and the aethalometer) seems not to

affect our data as the closure is always very good. Concerning the few points in Fig.4 with very small extinctions (less than 20 Mm⁻¹) the nephelometer+aethalometer extinction was slightly larger than the CAPS (less than 10% difference, which is within the instrument's uncertainties). Any possible effect of RH is however difficult to investigate due to the limited RH range in our measurements.

Line 382 – change to ‘...serve two purposes.’

The text was changed accordingly.

Line 386 – change to ‘...on relative amounts of particle absorption...’

The text was changed accordingly.

Line 407-408 – could cite Lack et al (2008) here – they saw enhanced absorption for filter-based measurements when more organic was present (for PSAP not aethalometer, but I imagine there could be a similar effect).

The suggested reference was added to the text.

Line 412-414 – it should be relatively straightforward (although admittedly annoying– sorry!) to recalculate results for MAAP at 630 nm to see how much of a role this wavelength discrepancy might play. I see from the acknowledgements that Andreas Petzold advised on this paper – perhaps ask him what he thinks about the MAAP measurement wavelength value.

We evaluated the impact of the exact wavelength on the retrieved C_{ref} by assuming 637 nm as the nominal MAAP wavelength and by using this value to extrapolate the absorption coefficient at 660 nm. We then used this new value to estimate C_{ref} . As expected, using 637 nm determines an increase in C_{ref} at 660 nm. This increase is +8–14% for mineral dust, +3% for kaolinite, and +3–15% for ambient air aerosols, independently of the used formulation for C_{ref} calculation (C2010, W2003, or C_{ref}^*).

In order to add this information in the main text we added the following text:

Sect. 2: “An estimate of the change in the obtained C_{ref} due to the change in MAAP nominal wavelength from 670 to 637 nm is reported in Sect. 4.2;”

Sect. 4.2: “If the wavelength of 637 nm is assumed for the MAAP instead of 670 nm, as suggested by Müller et al. (2011), the average C_{ref} at 660 nm would increase by up to ~15% for dust and ambient air (2.17 ± 0.19 and 2.48 ± 0.41 , respectively) and ~3% for kaolinite (2.40 ± 0.02).”

Line 424 – change to ‘...particles, and may be linked...’

The text was changed accordingly.

Line 426 – delete ‘In correspondence,’

The text was changed accordingly.

Line 435 – [comment – interesting that kaolinite has a significantly different absorption Angstrom exponent than dust. Isn't it often used as a surrogate for dust? Does this have any implications?

First; we found some errors in the text and numbers between lines 432-436, which we rewrote as: “The α_E (shown in Fig.2) was ~0 for kaolinite, varied between about 0 and 2 for mineral dust aerosols, and between 0.5 and 2.5 for ambient air, indicating particles with

variable sizes, both the sub-micron and the super-micron fractions. The absorption Ångström coefficient α_A obtained from aethalometer data was between 2.2 and 4 for dust, between 1 and 1.5 for kaolinite and between 0.5 and 1.5 for ambient air aerosols. “

To answer to your comment: yes, kaolinite is usually used as a surrogate of dust and this may lead to large uncertainties due to the differences in the size distribution and the composition between the two, which affect their absorbing behaviour, as we can see here for example in relation to the absorption Ångström coefficient α_A . We decided however not to stress this point in the manuscript since any comment or conclusion should deserve a more systematic study, which was not the case for this paper.

Line 442 – change to ‘In contrast, no dependence of C_{ref} on $De_{eff,fine}$ is found ($R^2 \leq 0.44$, not shown).’

The text was changed accordingly.

Line 454++ change to ‘Using these values of C_{ref} , the dust absorption coefficient estimated by the aethalometer will be about 2% (450 nm) and 11% (660 nm) higher than obtained...’

The text was changed accordingly.

Line 474 – delete ‘, even if beyond the scope of the paper,’

The text was changed accordingly.

Line 483-484 – change to ‘This trend was only observed when the entire dataset was considered, but not if the dataset was limited to just the dust observations, making it difficult to draw clear conclusions.’

The text was changed accordingly.

Line 485 change ‘...of C_{ref} is required...’

The text was changed accordingly.

Line 733 (and line 794) – change to ‘...(referred to as $R(C_{2010})$)...’

The text was changed accordingly.

Line 738 (and line 818) – change to ‘...kaolinite occurred between the...’

The text was changed accordingly.

Table 1 – where do these uncertainty values come from? There are more recent (better!) references for the nephelometer uncertainty (e.g., Sherman et al 2015 – see their supplemental materials).

The reference by Sherman was added in Table 1 together with their estimated uncertainty of ~9% on the nephelometer scattering coefficient.

Figure 5 – why are f values so different for niger 1 and niger 2 and does this have an effect on results? Suggests results aren’t totally reproducible.

The estimate of f values for Niger 1 and Niger 2 was 1.03 and 1.08 respectively, which corresponds to ~5% change. Even if not perfect, we consider these values sufficiently in accordance to prove the reproducibility of the results.

Figure 8d (lower right) should the word 'niger 1' be in the figure legend? If so, there should be a space between it and (W2003)

The plot was corrected.

General comment - A paper that might be of interest (if you haven't seen it) is Engelbrecht et al (2016) which has optical properties (e.g., SSA) for a bunch of different types of dust (i.e., dust from many different locations). I don't think you need to cite it (though you could). They used a photoacoustic instrument with a reciprocating nephelometer to obtain dust SSA values. If you and they have any overlapping dust samples it'd be nice to show/mention that the aethalometer had a similar response to dust as the photoacoustic since it's much simpler/cheaper to operate an aethalometer than a photoacoustic. Filter-based absorption instruments are often looked down on by some segments of the measurement community.

Only for China, Arizona, and Australia we found overlapping dust samples between our study and Engelbrecht et al. (2016). For these samples the comparison was quite good, despite the different wavelengths used in the two analyses. We included this comparison in the paper, with the following lines in Sect. 4.3: "In particular, our results for China, Arizona, and Australia samples are in line with published values by Engelbrecht et al. (2016), who used a photoacoustic instrument to measure absorption of re-suspended dust aerosols. This would suggest the similar performances of the aethalometer compared to the photoacoustic technique. The SSA for kaolinite was 0.96–0.97 at 450 and 660 nm, in agreement with Utry et al. (2017) also using a photoacoustic method to measure absorption (0.97 and 0.99 (± 0.04) at 450 and 635 nm, respectively)."

References

- Engelbrecht et al (2016) Atmos. Chem. Phys, 16, 10809, 2016
Lack et al (2008) Aerosol Science and Technology, 42:1033–1041, 2008
Petzold et al (2013) Atmos. Chem. Phys., 13, 8365–8379, 2013
Sherman et al (2015) Atmos. Chem. Phys., 15, 12487–12517, 2015

Referee #3

This is a very interesting manuscript of great importance for measuring mineral dust absorption coefficients with the AE31 aethalometer. It should be accepted for publication in AMT after the following comments have been taken into account.

1. Would these results be relevant to the currently sold AE33 aethalometer and would the authors expect the same C_{ref} values?

The authors do not have a detailed knowledge of the new AE33 model and its performances, however given that the principle of measure is the same of the AE31 model the obtained C_{ref} should work well also with the aethalometer AE33. The main change in the AE33 model consists in the use of the dual-spot technology to reduce the loading effect, while not specific improvements were reported concerning the multiple scattering effect.

2. L9-10: The abstract needs a better definition of C_{ref} .

The following definition of C_{ref} has been added into the abstract: " C_{ref} is an empirical constant used to correct the aerosol absorption coefficient measurements for the multiple scattering artefact of the aethalometer, i.e. the filter fibres on which aerosols are deposited scatter light and this is miscounted as absorption."

3. L83 and elsewhere: "Shadowing Effect": While this has a meaning in the geometric optics regime ($x \gg 1$), it is completely meaningless for particle sizes comparable to or smaller than the wavelength. As this study encompasses both cases, a different expression (e.g., loading effect) should be used.

"Shadowing effect" was replaced with "Loading effect" throughout the paper.

4. As three different kinds of aerosol absorption measurements (AE31, MAAP, difference method) form the core of this manuscript, general references on absorption measurements should be added such as the two major reviews of atmospheric and aerosol absorption by Horvath (1993) and Moosmüller et al. (2009).

The following sentence was added in the introduction of the paper: "General reviews on aerosol absorption measurements and their applications are provided by Horvath (1993) and Moosmüller et al. (2009)."

5. L239-255: The Nephelometer truncation correction needs error estimations for both methods. Also were the particles sampled approximately spherical (SEM) images and what errors are expected from the assumption of spherical dust particles.

The truncation correction uncertainty was calculated as following: (i) for the Anderson and Ogren (1998) method we applied the error propagation formula taking into account the uncertainty on the parameters used for correction as provided by these authors their paper; (ii) for the method using Mie calculations what we did was to perform the truncation correction by considering the uncorrected nephelometer scattering coefficients \pm their uncertainty of $\sim 9\%$ and we calculated the deviation of the obtained C_{trunc} in these cases. For both methods the calculated uncertainty was $< 3\%$.

The following sentence was added in Sect. 3.4.2: "For both approaches (Anderson and Ogren (1998) correction and Mie calculations) the uncertainty on the truncation correction was estimated to be less than 3%."

Concerning the impact of the particle shape, it is very difficult to estimate an uncertainty associated to this issue without an accurate measure of the particle shape, which indeed was not realised for this study. As shown by Mishchenko et al. (1997) for the T-matrix theory, for example, the phase function of non-spherical particles is strongly sensitive to the particle aspect ratio (i.e. the ratio of the larger to the shorter dust dimensions). Chou et al. (2008) has shown that the aspect ratio of dust may vary in the wide range 1 to 5, which means that either the dust shape is accurately characterized (which was not the case in this study), or the uncertainties due to the fact of using a wrong aspect ratio in the calculations risk to be comparable or even larger than the uncertainties due to the use of Mie theory. Anyhow, being C_{trunc} the ratio of two integrated quantities (the scattering at $0-180^\circ$ and $7-170^\circ$) we would not expect a large variation compared to the spherical case. As a simple calculation to prove this, we used the phase function in Fig. 1 by Mishchenko et al. (1997) for spherical dust and for oblate spheroids with an aspect ratio of 2.4 (very aspherical particle) and we calculated the C_{trunc} as the ratio of the integrated phase functions between $0-180^\circ$ and $7-170^\circ$ in the two cases. The curves by Mishchenko et al. refer to 443 nm and a refractive index of

1.53-0.0085i. The obtained C_{trunc} varied less than 1% between the spherical and spheroid cases, thus showing the very low sensitivity of the truncation correction to the particle shape.

Mishchenko, M. I., L. D. Travis, R. A. Kahn, and R. A. West, Modeling phase functions for dustlike tropospheric aerosols using a shape mixture of randomly oriented polydisperse spheroids, *J. Geophys. Res.*, 102, 16831–16848, 1997.

Chou, C., P. Formenti, M. Maille, P. Ausset, G. Helas, M. Harrison, and S. Osborne, Size distribution, shape, and composition of mineral dust aerosols collected during the African Monsoon Multidisciplinary Analysis Special Observation Period 0: Dust and Biomass-Burning Experiment field campaign in Niger, January 2006, *J. Geophys. Res.*, 113, D00C10, doi:10.1029/2008JD009897, 2008.

6. L374-375: “The wide range of [SSA] values indicates the occurrence of particles with very different absorption properties, henceforth chemical composition.” It either indicates different chemical composition (or complex refractive index) and/or different size distribution as SSA strongly depends on both (e.g., Moosmuller and Arnott, 2009).

The text was changed following the reviewer’s suggestion.

7. L415-427: When discussing particle size distributions, please always clarify if you are talking about number size or volume (mass) size distribution.

The text was changed accordingly.

8. L457: “Given that the maximum intensity of the solar spectrum occurs at about 700 nm,...” I always thought that the maximum intensity (per wavelength interval) occurred around 500 nm. Please explain!

This was changed in “Given that the median of the solar spectrum occurs at about 700 nm...”. The median refers to the energy of the solar spectrum.

9. Some reference citations are inappropriate. For example, replace (Sokolik et al., 1999; L40) with (Sokolik and Toon, 1999; L40). Please check others!

The Sokolik et al. (1999) reference was changed as suggested by the reviewer. In addition, the Petzold et al. (2004) reference was modified in Petzold et al. (2005) both in Sect. 2 and in Table 1, and finally the Utry et al. (2016) was modified in Utry et al. (2017) in Sect.4.3.

10. P. 15-18: REFERENCES. This listing is incomplete and needs to be checked and completed! For example, Highwood and Ryder, 2014 (L38), Arnott et al., 2005 (L86), Petzold et al., 2004 (L114) are missing in the list of references.

The reference list was checked and completed.

REFERENCES

Horvath, H. (1993). "Atmospheric Light Absorption - A Review." *Atmospheric Environment* 27A(3): 293-317.

Moosmuller, H., R. K. Chakrabarty and W. P. Arnott (2009). "Aerosol Light Absorption : A Review." *Journal of Quantitative Spectroscopy & Radiative Transfer* 110(11): 844-878.

Moosmuller, H. and W. P. Arnott (2009). Particle Optics in the Rayleigh Regime. *J. Air & Waste Manage. Assoc.*, 59, 1028-1031.

Aethalometer multiple scattering correction C_{ref} for mineral dust aerosols

Claudia Di Biagio¹, Paola Formenti¹, Mathieu Cazaunau¹, Edouard Pangui¹, Nicholas Marchand², and Jean-François Doussin¹

¹ Laboratoire Interuniversitaire des Systèmes Atmosphériques (LISA), UMR 7583, CNRS, Université Paris Est Créteil et Université Paris Diderot, Institut Pierre et Simon Laplace, Créteil, France

² Aix Marseille Université, CNRS, LCE, Marseille, France

Correspondence to: C. Di Biagio (cldibiagio@gmail.com) and P. Formenti (paola.formenti@lisa.u-pec.fr)

Mis en forme : Centré, Espace Après : 6 pt, Interligne : 1.5 ligne, Paragraphes solidaires

Mis en forme : Police : (Par défaut) Arial, 9 pt, Français (France)

Abstract

In this study we provide a first estimate of the aethalometer multiple scattering correction C_{ref} for mineral dust aerosols. C_{ref} is an empirical constant used to correct the aerosol absorption coefficient measurements for the multiple scattering artefact of the aethalometer, i.e. the filter fibres on which aerosols are deposited scatter light and this is miscounted as absorption. The C_{ref} at 450 and 660 nm was obtained from the direct comparison of aethalometer data (Magee Sci. AE31) with the absorption coefficient calculated as the difference between the extinction and scattering coefficients measured by a Cavity Attenuated Phase Shift Extinction analyzers (CAPS PMex) and a nephelometer respectively at 450 nm and the absorption coefficient from a MAAP (Multi-Angle Absorption Photometer) at 660 nm. Measurements were performed on seven dust aerosol samples generated in the laboratory by the mechanical shaking of natural parent soils issued from different source regions worldwide. The single scattering albedo (SSA) at 450 and 660 nm and the size distribution of the aerosols were also measured.

Mis en forme : Indice

C_{ref} for mineral dust varies between 1.81 and 2.56 for a SSA of 0.85–0.96 at 450 nm and between 1.75 and 2.28 for a SSA of 0.98–0.99 at 660 nm. The calculated mean and one standard deviation C_{ref} for dust is 2.09 (\pm 0.22) at 450 nm and 1.92 (\pm 0.17) at 660 nm. With this new C_{ref} the dust absorption coefficient by aethalometer is about 2% (450 nm) and 11% (660 nm) higher than that obtained by using $C_{ref}=2.14$ at both 450 and 660 nm, as usually assumed in the literature. This difference induces up to 3% change in the dust SSA at 660 nm. The C_{ref} seems independent of the particle fine and coarse size fractions, and so the obtained C_{ref} can be applied to dust both close to sources and following transport. Additional experiments performed with pure kaolinite mineral and polluted ambient aerosols indicate a C_{ref} of 2.49 (\pm 0.02) and 2.32 (\pm 0.01) at 450 and 660 nm respectively (SSA=0.96–0.97) for kaolinite, and a C_{ref} of 2.32 (\pm 0.36) at 450 nm and 2.32 (\pm 0.35) at 660 nm for pollution aerosols (SSA=0.62–0.87 at 450 nm and 0.42–0.76 at 660 nm).

37
38
39
40
41
42
43
44
45
46
47
48
49
50
51
52
53
54
55
56
57
58
59
60
61
62
63
64
65
66
67
68
69
70
71
72
73

1. Introduction

Abundant and widespread in the atmosphere, mineral dust strongly contributes to the global and regional direct radiative effect and climate forcing (Highwood and Ryder, 2014; Miller et al., 2014). Mineral dust interacts through processes of scattering and absorption with both incoming shortwave radiation and outgoing terrestrial longwave radiation (Sokolik ~~et al.~~ and Toon, 1999). ~~As for today~~Currently, the evaluation of the direct effect of mineral dust and its climate implications is still limited by the knowledge of the intensity of the dust absorption in the shortwave spectral range (Miller et al., 2004; Balkanski et al., 2007; Solmon et al., 2008; Jin et al., 2016), represented by the light absorption coefficient (β_{abs} , units of Mm^{-1}). The absorption coefficient of mineral dust accounts for less than ~10-20% of its total shortwave extinction, where it shows a pronounced spectral variation (Catrall et al., 2003; Redmond et al., 2010). The highest dust absorption occurs in the UV-VIS region of the spectrum, while it levels off to null values towards the near IR (Caponi et al., 2017). As a result, its single scattering albedo (SSA), i.e. the ratio of the aerosol scattering (β_{sca}) to extinction ($\beta_{\text{ext}} = \beta_{\text{sca}} + \beta_{\text{abs}}$) coefficient, increases from values of ~0.80-0.90 at 370 nm to values of ~0.95-0.99 at 950 nm (e.g., Schladitz et al., 2009; Redmond et al., 2010; Formenti et al., 2011; Ryder et al., 2013).

Given its relatively high SSA, mineral dust can be considered as weakly absorbing in the shortwave. This is particularly true ~~if~~when compared to other aerosol species, ~~such as soot~~, for which the SSA in the visible may be as low as 0.2 (Bergstrom et al., 2007). Nonetheless, because of its elevated atmospheric concentration (~100-~~100000~~ $\mu\text{g m}^{-3}$ close to sources and ~0.1-~~100~~ $\mu\text{g m}^{-3}$ after mid- to intercontinental transport; e.g., Goudie and Middleton, 2006; Kandler et al., 2009; Querol et al., 2009; Denjean et al., 2016a), light absorption by mineral dust can be comparable to that of soot both at regional and global scales (Reddy et al., 2005; Caponi et al., 2017). Under very intense dust episodes, dust may absorb up to ~150 Wm^{-2} of incoming solar radiation (Slingo et al., 2006; di Sarra et al., 2011), inducing a remarkable warming of the atmospheric layer. This strong warming can alter the atmospheric structure and stability (Heinold et al., 2008), with a possible influence on the atmospheric dynamics and meteorological fields (Pérez et al., 2006). By its direct shortwave effect dust also affects the position of the Inter Tropical Convergence Zone, which in turn influences the Western African Monsoon and modifies the pattern and intensity of rainfall over Northern Africa and the Sahel (Yoshioka et al., 2007). Nonetheless, the extent of the dust effect and its implications critically depend on the exact amount of absorbed shortwave radiation. Solmon et al. (2008), for example, showed that a small change (5%) in the shortwave SSA of dust may modify the effect of dust on the Western African Monsoon, moving from a reduction to an increase of precipitation over the Sahel.

74 The accurate estimation of the dust absorption over the whole shortwave range is therefore
75 necessary to properly assess its direct radiative effect and climate implications. One instrument used
76 to obtain measuring the aerosol-light absorption from the UV to near IR range is the aethalometer
77 (Magee Sci. AE31 model, Hansen et al., 1984; Arnott et al., 2005), operating at seven wavelengths in
78 the 370–950 nm range. The aethalometer reports is used to measure the equivalent black carbon
79 mass concentration but the spectral absorption by aerosols can be also calculated. Given its large
80 spectral interval, the aethalometer has been used in the past to investigate the spectral dependence
81 of dust absorption (Fialho et al., 2005; Formenti et al., 2011), as well as the absorption by many
82 aerosol types in different environments (Sandradewi et al., 2008; Segura et al., 2014; Di Biagio et al.,
83 2016; Backman et al., 2016). General reviews on aerosol absorption measurements and their
84 applications are provided by Horvath (1993) and Moosmüller et al. (2009).

85 The working principle of the aethalometer, a filter-based instrument, consists in measuring the
86 attenuation through an aerosol-laden quartz filter according to the Beer-Lambert law, used then to
87 derive the spectral attenuation coefficient (β_{ATT}) of the deposited particles (Hansen et al., 1984). The
88 “true” spectral aerosol absorption coefficient (β_{abs}) is proportional but lower than β_{ATT} (Weingartner et
89 al., 2003; Collaud Coen et al., 2010; hereinafter referred as W2003 and C2010), because β_{ATT} is
90 enhanced by (i) aerosol scattering towards directions different from that of the detector (scattering
91 effect); (ii) gradual accumulation of absorbing particles on the loaded filter, thus reducing the optical
92 path (shadowing-loading effect); (iii) multiple scattering of the light beam by the filter fibres, increasing
93 the optical path (multiple scattering effect).

94 Empirical formulations of the scattering and shadowing-loading effects are available in the literature
95 and permit the correction of aethalometer data for these artefacts (W2003; Arnott et al., 2005; Schmid
96 et al., 2006; Virkkula et al., 2007; C2010). The correction of the multiple scattering effect, however
97 requires the knowledge of a correction factor C_{ref} , which needs to be directly estimated by comparison
98 of aethalometer data against reference absorption measurements (W2003; C2010).

99 Currently data for C_{ref} are available for soot particles ($C_{\text{ref}}=2.1\text{--}2.2$ at 660 nm, W2003), internally and
100 externally mixed soot particles and organic material ($C_{\text{ref}}=2.3\text{--}3.9$, W2003), and ambient aerosols
101 collected in Europe and Amazonia ($C_{\text{ref}}=2.6\text{--}4.8$, C2010; $C_{\text{ref}}=4.9\text{--}6.3$, Saturno et al., 2016) and in the
102 Arctic ($C_{\text{ref}}=3.1$, Backman et al., 2016). The value most often used in the literature is 2.14 (± 0.21),
103 assumed as wavelength-independent (e.g., Sandradewi et al., 2008; Formenti et al., 2011; Di Biagio
104 2016), which corresponds to the mean of observations at 660 nm for soot aerosols (W2003). Both
105 W2003 and C2010, however, found a dependence of C_{ref} on the aerosol single scattering albedo, with
106 C_{ref} decreasing for increasing SSA. So Thus, the value of 2.14 obtained for highly absorbing soot
107 (SSA~0.2 in the visible) may not be appropriate for weakly absorbing mineral dust.

108 Henceforth, in this work we present the experimental estimate of an optimized C_{ref} for mineral dust
109 aerosols at 450 and 660 nm obtained from a laboratory-based intercomparison study. Experiments
110 were conducted on seven dust aerosol samples generated by the mechanical shaking of natural
111 parent soils. Control experiments on pure kaolinite mineral, ambient aerosols sampled in the polluted

112 environment of the suburbs of Paris, and purely scattering ammonium sulfate, were also performed to
113 investigate the dependence of C_{ref} on the aerosol single scattering albedo.

114

115 2. Experimental set-up

116 The experimental set-up used for the intercomparison study is shown in Fig. 1. [Instrumental details](#)
117 [and uncertainties are summarized in Table 1.](#)

118 The following measurements were performed from a 8-port glass manifold (~1 L volume):

119 - the absorption coefficient (β_{abs}) by a 7-wavelength aethalometer (Magee Sci., model AE31
120 working at 370, 470, 520, 590, 660, 880, 950 nm; flowrate 8 L min⁻¹, 2-min resolution) and a MAAP
121 (Multi-Angle Absorption Photometer, Thermo Sci., model 5012 working at 670 nm; flowrate 8 L
122 min⁻¹, 1-min resolution). Unlike the aethalometer, the MAAP measures the transmitted light from
123 the aerosol-laden filter and also the backscattered light at two angles (135° and 165°) (Petzold et
124 al., 2005⁴). Backscattering measurements are used to constrain the scattering fraction of the
125 measured attenuation that would erroneously be interpreted as absorption. The aerosol absorption
126 coefficient for the MAAP is obtained from a radiative transfer scheme taking into account the
127 multiple scattering in the filter and the scattering effect, without requiring any further adjustment
128 (Petzold and Schönlinner, 2004). The MAAP is commonly assumed to provide the most reliable
129 [filter-based](#) direct estimate of the aerosol absorption coefficient at a single wavelength (Andreae
130 and Gelécsér 2006). In this study we assume for the MAAP the manufacturer's reported
131 wavelength of 670 nm, [even if although](#) Müller et al. (2011) measured for this instrument a
132 wavelength of 637 nm. [An estimate of the change in the obtained \$C_{ref}\$ due to the change in MAAP](#)
133 [nominal wavelength from 670 to 637 nm is reported in Sect. 4.2;](#)

Mis en forme : Indice

134 - the scattering coefficient (β_{sca}) in the 7-170° angular range by a 3-wavelength nephelometer (TSI
135 Inc., model 3563 working at 450, 550 and 700 nm; flowrate 18 L min⁻¹, 1-s resolution);

136 - the extinction coefficient (β_{ext}) by two Cavity Attenuated Phase Shift Extinction analyzers (CAPS
137 PMex by Aerodyne, one working at 450 nm and the other at 630 nm; flowrate 0.85 L min⁻¹, 1-s
138 resolution);

139 - the particle number size distribution (dN/dlogD) by a scanning mobility particle sizer, SMPS, (TSI
140 Inc., DMA Model 3080, CPC Model 3772; operated at 2.0/0.2 L min⁻¹ sheath/aerosol flow rates; 3-
141 min resolution) and an optical particle counter, OPC, (Grimm Inc., model 1.109, 655 nm operating
142 wavelength; flowrate 1.2 L min⁻¹, 6-s resolution). The SMPS measures the aerosol number
143 concentration in the electrical mobility diameter (D_m) range 0.019–0.882 μm , and the OPC
144 measures in the optical equivalent diameter (D_{opt}) range 0.25–32 μm .

145 [Instrumental details are summarized in Table 1.](#)

146 Sampling lines from the manifold to the instruments were made of conductive silicone tubing (TSI Inc.,
147 $6.4 \cdot 10^{-3}$ m diameter) to minimize particle loss by electrostatic deposition. They were designed to be as
148 straight and as short as possible. Their length, varying between 0.3 and 0.7 m, was adjusted based

149 on the flowrate of each instrument to ensure an equivalent particle loss, so that the same aerosol size
150 distribution ~~could be assumed asis in~~ input ~~for to all the different~~ instruments. Particular care was
151 given to ensure the same aerosol size at the input of the aethalometer and the MAAP. To this end, as
152 illustrated in Fig. 1, the two instruments sampled air from the same manifold exit line, and also the
153 same sampling flow rate was set for the two instruments (8 L min⁻¹). Particle loss calculations were
154 performed with the Particle Loss Calculator (PLC) software (von der Weiden et al., 2009).

155 Aerosols were generated in three ways:

156 - mineral dust was generated by mechanical shaking as described and validated in Di Biagio et al.
157 (2014, 2017). About 3 gr of soil sample (sieved at 1000 µm and dried at 100°C) was placed in a
158 Büchner flask and shaken at 100 Hz by a sieve shaker (Retsch AS200). The dust was injected in the
159 manifold by a flow of N₂ at 3.5 L min⁻¹ through a single-stage impactor used to eliminate particles
160 larger than about 20 µm, which could be preferentially sampled by the instruments with the highest
161 flow rate. Pure N₂ was added to the aerosol flow to make the injection flow equal to the total sampling
162 flow by instruments connected to the manifold (about 38 L min⁻¹);

163 - ammonium sulfate (Sigma-Aldrich 99.999% purity, 0.03 M solution in ultrapure water) and kaolinite
164 particles (Source Clay Repository KGa-2, 0.05 M solution in ultrapure water) were generated by a
165 constant flow atomizer (TSI, model 3075) operated at 3 L min⁻¹ and coupled with a diffusion drier (TSI,
166 model 3062). As for dust, pure N₂ was added to the aerosol flow to equalize the total sampling flow;

167 - ambient pollution aerosols were sampled by opening the manifold to the exterior ambient air.
168 Ambient aerosols were not dried before entering the manifold. Sampling was performed at the
169 University Paris-Est Creteil, in the suburbs of Paris, at the ground floor of the University building,
170 which is close to a main local road (~20 m) and to the A86 highway (~200 m).

171

172 3. Strategy for data analysis

173 The aethalometer spectral attenuation coefficient $\beta_{ATT}(\lambda)$ is related to the measured attenuation
174 $ATT(\lambda)$ through the following formula:

$$175 \quad \beta_{ATT}(\lambda) = \frac{\Delta ATT(\lambda) A}{\Delta t V} \quad (1)$$

176 where A is the area of the aerosol collection spot (0.5 ± 0.1) cm² and V the air sampled volume (0.016
177 m³ over 2-min integration time). $\Delta ATT(\lambda)/\Delta t$ in Eq. (1) can be calculated as the linear fit of the
178 measured attenuation as a function of time.

179 The spectral attenuation coefficient $\beta_{ATT}(\lambda)$ measured by the aethalometer is related to the targeted
180 absorption coefficient $\beta_{abs}(\lambda)$ by the following formula (C2010):

$$181 \quad \beta_{abs}(\lambda) = \frac{\beta_{ATT}(\lambda) - \alpha(\lambda)\beta_{sca}(\lambda)}{R \cdot C_{ref}} \quad (2)$$

182 where the different terms parametrise different instrument artefacts:

183 - the scattering effect $\alpha(\lambda)\beta_{\text{sca}}(\lambda)$, that is, the amount of scattered radiation by the aerosols deposited
 184 on the filter that is miscounted as absorption, where $\alpha(\lambda)$ is a wavelength-dependent proportionality
 185 constant and $\beta_{\text{sca}}(\lambda)$ is the aerosol spectral scattering coefficient;

186 - the **shadowing-loading** effect R, representing the artificial flattening of measured attenuation with
 187 time due to the gradual accumulation of absorbing particles on the loaded filter;

188 - the multiple scattering C_{ref} , representing multiple scattering of the light beam by the filter fibres.

189 The $\alpha(\lambda)$ term and R in Eq. (2) can be calculated through various empirical formulas reported in the
 190 literature (W2003, Arnott et al., 2005; Virkkula et al., 2007; Schmid et al., 2006; C2010). The
 191 determination of C_{ref} , instead, is the objective of our study.

192

193 3.1. Scattering effect correction

194 Arnott et al. (2005) provide for $\alpha(\lambda)$ the following formulation:

$$195 \quad \alpha(\lambda) = A^{d-1} \cdot c \cdot \lambda^{-\alpha_s(d-1)} \quad (3)$$

196 where the A and α_s terms are obtained from the power-law fit of $\beta_{\text{sca}}(\lambda)$ versus λ , and the c and d
 197 terms can be determined from the power-law fit of the attenuation $\beta_{\text{ATT}}(\lambda)$ versus the scattering $\beta_{\text{sca}}(\lambda)$
 198 coefficient as

$$199 \quad \beta_{\text{sca}}(\lambda) = A\lambda^{-\alpha_s} \quad (4)$$

$$200 \quad \beta_{\text{ATT}}(\lambda) = c\beta_{\text{sca}}(\lambda)^d \quad (5)$$

201 3.2. Shadowing-Loading effect correction

202 Two formulations for the **shadowing-loading** effect correction R are proposed by W2003 and C2010:

$$203 \quad R(\text{W2003})(\lambda) = \left(\frac{1}{f(\lambda)} - 1 \right) \frac{\ln(\text{ATT}(\lambda)) - \ln(10\%)}{\ln(50\%) - \ln(10\%)} + 1 \quad (6a)$$

$$204 \quad R(\text{C2010})(\lambda) = \left(\frac{1}{f(\lambda)} - 1 \right) \frac{\text{ATT}(\lambda)}{50\%} + 1 \quad (6b)$$

205 The factor $f(\lambda)$ represents the dependence of the **shadowing-loading** effect on the aerosol absorption.
 206 This dependence is parametrized by the aerosol single scattering albedo $\text{SSA}(\lambda)$ in the form of

$$207 \quad f(\lambda) = a(1 - \text{SSA}(\lambda)) + 1 \quad (7)$$

208 where a, equal to 0.85 in W2003 and 0.74 in C2010, is obtained as the slope of the linear fit between
 209 the attenuation coefficient β_{ATT} normalized to its value at 10% attenuation ($\beta_{\text{ATT}}/\beta_{10\%}$) and the natural
 210 logarithm of the measured attenuation $\ln(\text{ATT}(\lambda))$.

211 3.3. Multiple scattering correction

212 For the determination of C_{ref} only β_{ATT} and R are required. Henceforth in this work, attenuation data
 213 from the aethalometer were corrected for the shadowing-loading effect R but not for the scattering
 214 term $\alpha(\lambda)\beta_{sca}(\lambda)$. Three different formulations of C_{ref} were therefore considered:

$$215 \quad C_{ref}^*(\lambda) = \frac{\beta_{ATT}(\lambda)}{\beta_{abs-ref}(\lambda)} \quad (8a)$$

$$216 \quad C_{ref}(W2003)(\lambda) = \frac{1}{\beta_{abs-ref}(\lambda)} \frac{\beta_{ATT}(\lambda)}{R(W2003)(\lambda)} \quad (8b)$$

$$217 \quad C_{ref}(C2010)(\lambda) = \frac{1}{\beta_{abs-ref}(\lambda)} \frac{\beta_{ATT}(\lambda)}{R(C2010)(\lambda)} \quad (8c)$$

218 The $\beta_{abs-ref}$ term in Eq. 8a-8c represents the reference absorption coefficient estimated from
 219 independent measurements. C_{ref}^* does not take into account the shadowing-loading effect correction
 220 in aethalometer data, as done by Schmid et al. (2006). $C_{ref}(W2003)$ and $C_{ref}(C2010)$ take this
 221 correction into account, by using the $R(W2003)$ and the $R(C2010)$ parametrisations, respectively. The
 222 spectral $\beta_{ATT}/R(C2010)$ was used to calculate the absorption Ångström exponent (α_A). Note that in this
 223 work we considered, for each experiment, only data corresponding to $ATT < 20\%$ to calculate β_{ATT}
 224 ($R^2 > 0.99$ for the $\Delta ATT/\Delta t$ fits in all cases, see Eq. (1)). This threshold was fixed based on two
 225 requirements: first, we limited our data analysis to points with low attenuation in order to account
 226 almost exclusively for the scattering by the filter fibers in the C_{ref} calculation and not for the scattering
 227 from aerosol particles embedded in the filter. This choice was done also for consistency with the
 228 literature, since both W2003 and C2010 relate C_{ref} to $ATT \sim 10\%$. Second, this choice ensured that
 229 enough data points were available for analysis regardless of the aerosol type, in particular for ambient
 230 aerosols, for which attenuation rapidly exceeded 10%.

231 3.4. Determination of reference absorption coefficient and single scattering albedo

232 The reference absorption coefficient $\beta_{abs-ref}$ in Eq. 8a-8c was obtained in different ways depending on
 233 wavelength. At 450 nm, $\beta_{abs-ref}$ was obtained with the “extinction minus scattering” approach by using
 234 the CAPS measurements for extinction and the nephelometer measurements for scattering. At 660
 235 nm, $\beta_{abs-ref}$ was extrapolated from MAAP measurements at 670 nm.

236 3.4.1. Direct determination of reference absorption coefficient at 660 nm from the MAAP

237 The reference absorption coefficient $\beta_{abs-ref}$ at 660 nm was obtained by the MAAP measurement at
 238 670 nm. The MAAP attenuation (ATT) at 670 nm is estimated from the measured transmission (T)
 239 and retrieved single scattering albedo of the aerosol-filter layer (SSA_0 , from the inversion algorithm)
 240 as

$$241 \quad ATT(670) = (1 - SSA_0) \cdot \ln T \cdot 100 \quad (9)$$

242 Equation (1) is applied to estimate the absorption coefficient at 670 nm from $ATT(670)$. The area of
 243 the aerosol collection spot is 2 cm^2 and the sampled volume is 0.008 m^3 over 1-min integration time.

244 The absorption coefficient of the MAAP was extrapolated to the 660 nm wavelength by using the
245 absorption Ångström exponent α_A calculated from aethalometer data.

246 **3.4.2. Indirect determination of reference absorption coefficient at 450 nm: "extinction minus 247 scattering" approach**

248 The reference absorption coefficient $\beta_{\text{abs-ref}}$ at 450 nm was calculated as the difference between the
249 extinction and scattering coefficient from the CAPS and the nephelometer.

250 The extinction coefficient β_{ext} at 450 and 630 nm was measured directly by the two CAPS analyzers
251 without additional corrections (Massoli et al., 2010). The spectral β_{ext} was used to calculate the
252 extinction Ångström exponent (α_E), applied then to extrapolate β_{ext} at 660 nm.

253 The scattering coefficient β_{sca} at 450, 550, and 700 nm measured by the nephelometer between 7 and
254 170° was corrected for the size-dependent angular truncation of the sensing volume to report it to the
255 full angular range 0°-180° (Anderson and Ogren, 1998). Two different approaches were used: for sub-
256 micrometric ammonium sulfate, the correction proposed by Anderson and Ogren (1998) was applied,
257 while for aerosols with a significant coarse fraction (dust, ambient air and kaolinite), the truncation
258 correction was estimated by optical calculations according to the Mie theory for homogeneous
259 spherical particles using as input the measured number size distribution. In the calculations the real
260 and the imaginary parts of the complex refractive index m ($m=n-ik$, where n is the real part and k is
261 the imaginary part) were varied in the wide range 1.42–1.56 and 0.001–0.025*i* for dust (Di Biagio et
262 al., 2017), and 1.50–1.72 and 0.001–0.1*i* for ambient air (Di Biagio et al., 2016), while the value of
263 1.56-0.001*i* was assumed for kaolinite (Egan and Hilgeman, 1979; Utry et al., 2015). Then, n and k
264 were set to the values which reproduced the measured β_{sca} at 7-170°. The truncation correction factor
265 (C_{trunc}) was estimated as the ratio of the modelled β_{sca} at 0°-180° and 7°-170°. At the three
266 nephelometer wavelengths (450, 550, and 700 nm) the correction factor C_{trunc} varied in the range
267 1.03-1.06 for ammonium sulfate, 1.08-1.6 for dust, 1.03-1.05 for kaolinite, and 1.05-1.25 for ambient
268 air. For both approaches (Anderson and Ogren (1998) correction and Mie calculations) the
269 uncertainty on the truncation correction was estimated to be less than 3%. Once corrected for
270 truncation, the spectral β_{sca} was used to calculate the scattering Ångström exponent (α_S), which was
271 then applied ~~then~~ to extrapolate β_{sca} at 630 and 660 nm.

272 **3.4.3. Determination of the single scattering albedo (SSA)**

273 The aerosol single scattering albedo (SSA) represents the ratio of scattering to extinction. At 450 nm,
274 the SSA was estimated by nephelometer and CAPS data (Eq. 10), while at 660 nm CAPS data were
275 combined with MAAP observations (Eq. 11):

$$276 \quad \text{SSA}(450) = \frac{\beta_{\text{sca}}(450)_{\text{nephelometer}}}{\beta_{\text{ext}}(450)_{\text{CAPS}}} \quad (10)$$

$$277 \quad \text{SSA}(660) = \frac{\beta_{\text{ext}}(660)_{\text{CAPS}} - \beta_{\text{abs-MAAP}}(660)}{\beta_{\text{ext}}(660)_{\text{CAPS}}} \quad (11)$$

278

279 **3.5. Number size distribution and effective fine and coarse diameter**

280 The number size distribution was measured by a combination of SMPS and OPC observations. For
 281 the SMPS, corrections for particle loss by diffusion in the instrument tubing and the contribution of
 282 multiple-charged particles were performed using the SMPS software. The electrical mobility diameter
 283 measured by the SMPS can be converted to a geometrical diameter (D_g) by taking into account the
 284 particle dynamic shape factor (χ ; $D_g = D_m/\chi$). In this study, the SMPS showed a good agreement with
 285 OPC data for a shape factor $\chi=1$, which corresponds to spherical particles.

286 The OPC optical-equivalent nominal diameters were converted into sphere-equivalent geometrical
 287 diameters (D_g) by taking into account the aerosol complex refractive index. This consisted in
 288 recalculating the OPC calibration curve for different complex refractive index values. For dust
 289 aerosols the refractive index was varied in the range 1.47-1.53 (n) and 0.001-0.005i (k) following the
 290 literature (see Di Biagio et al., 2017) and D_g was set at the mean \pm one standard deviation of the
 291 values obtained for the different n and k. For kaolinite the OPC diameter conversion was performed
 292 by setting the refractive index at 1.56-0.001i. For ambient air the refractive index was set at 1.60-
 293 0.01i, a value that represents a medium absorbing urban polluted aerosol (see Di Biagio et al., 2016).
 294 The impact of humidity on the refractive index of ambient aerosols and associated changes OPC
 295 response are not taken into account. The relative humidity was always below 35% during ambient air
 296 measurements, which implies a very small particle growth. After conversion, the OPC diameter range
 297 became 0.28-18.0 μm for dust (taking into account the particle cut at $\sim 20 \mu\text{m}$ due to the use of the
 298 impactor), and 0.27-58.0 μm for kaolinite and 0.28-65.1 μm for ambient air (the impactor was not used
 299 in these cases). The uncertainty was $<15\%$ at all diameters.

300 The aerosol effective fine ($D_{\text{eff, fine}}$) and coarse ($D_{\text{eff, coarse}}$) diameter were estimated from OPC data as

301
$$D_{\text{eff}} = \frac{\int_{D_1}^{D_2} D_g^3 \frac{dN}{d\log D_g} d\log D_g}{\int_{D_1}^{D_2} D_g^2 \frac{dN}{d\log D_g} d\log D_g} \quad (12)$$

302 with $D_1=0.3 \mu\text{m}$ and $D_2=1 \mu\text{m}$ for the fine mode and $D_1=1 \mu\text{m}$ and $D_2=10 \mu\text{m}$ for the coarse mode.

303
$$D_{\text{eff, coarse}} = \frac{\int_{1\mu\text{m}}^{10\mu\text{m}} D_g^3 \frac{dN}{d\log D_g} d\log D_g}{\int_{1\mu\text{m}}^{10\mu\text{m}} D_g^2 \frac{dN}{d\log D_g} d\log D_g} \quad (13)$$

Mis en forme : Justifié
 Mis en forme : Indice
 Mis en forme : Indice

304 **3.6. Data integration and error analysis**

305 Aethalometer data were first processed at 2-min resolution to obtain the time evolution of the
 306 attenuation coefficients β_{ATT} and β_{ATT}/R . Data from the MAAP, CAPS, nephelometer, OPC and SMPS
 307 were averaged over 2-min to report them to the same resolution of the aethalometer.

308 Then the β_{ATT} and β_{ATT}/R were calculated over the whole duration of each experiment from Eq. (1)
 309 and (6). Corresponding averages of the reference absorption coefficient ($\beta_{\text{abs-ref}}$) were calculated for

310 each experiment and used to estimate C_{ref} . Experiment-averages of SSA, $D_{eff, fine}$, and $D_{eff, coarse}$ were
311 also calculated to relate to the obtained C_{ref} .

312 The uncertainty of C_{ref} was estimated with the error propagation formula by taking into account the
313 uncertainties on β_{ATT} , β_{ATT}/R , and the standard deviation of the averaged $\beta_{abs-ref}$ from the CAPS-
314 nephelometer and the MAAP. The uncertainty of β_{ATT} was estimated as the quadratic combination of
315 the uncertainty of the linear fit of ΔATT with respect to time and the uncertainties on the surface
316 deposit A. The uncertainty of β_{ATT}/R was estimated taking into account the uncertainty of β_{ATT} and
317 R. Uncertainties on β_{ATT} and β_{ATT}/R are both $\sim 20\%$.

318

319 4. Results

320 The time series of observations for all the experiments are shown in **Fig. 2** as 2-min averages. Seven
321 experiments were performed on mineral dust issued from six different areas in the Sahel (Niger),
322 Eastern Asia (China), North America (Arizona), Northern Africa (Tunisia), Australia, and Southern
323 Africa (Namibia), and on a kaolinite powder. Experiments were performed between the 3rd and the 9th
324 of November 2016 and lasted between 1 and 2 hours each. The experiment on Niger dust (labelled
325 as Niger 1 and Niger 2) were duplicated to test the repeatability of the obtained C_{ref} . Ambient air data
326 were collected between the 8th and the 14th November 2016 for a total of 7 hours of measurements.
327 Eight different periods characterized by little variation and different levels of SSA were selected in the
328 whole set of ambient air measurements. These are identified as ambient air 1 to 8. The summary of
329 information is provided in **Table 2**. SMPS data were available for ammonium sulfate and kaolinite
330 experiments, for one of the two Niger dust experiments (Niger 2), and for some of the ambient air
331 experiments. OPC measurements were performed for all experiments with the exception of the
332 ammonium sulfate.

333 4.1. Quality control data

334 Results of the ammonium sulfate control experiment (24 October 2016), used to test the
335 performances of the optical instruments, are illustrated in **Fig. 3**. As expected for this purely scattering
336 aerosol (Toon et al., 1976), the nephelometer scattering and the CAPS extinction at 450 and 630 nm
337 were in very good agreement (less than 4% difference) during the whole duration of the experiment.
338 This is well below the single instrument uncertainty of $\pm 9\%$ for the nephelometer (Sherman et al.,
339 2015) and $\pm 5\%$ for the CAPS (Massoli et al., 2010). This is further ~~explicated~~ demonstrated by the
340 scatterplot of their respective 10-minute averages, yielding a linear regression in the form of
341 $y=0.95x+5.1$ ($R^2=0.95$) at 450 nm and $y=1.01x-1.4$ ($R^2=0.98$) at 630 nm. The average β_{ext} at 450 and
342 630 nm from CAPS observations was $913 (\pm 52)$ and $424 (\pm 33) \text{ Mm}^{-1}$, respectively, while the average
343 β_{sca} was $921 (\pm 36)$ and $420 (\pm 17)$. This led to an average SSA of $1.01 (\pm 0.07)$ at 450 nm and $0.99 (\pm$
344 $0.07)$ at 630 nm.

345 The absorption coefficient, averaged over the duration of the experiment, was $0.10 (\pm 0.04) \text{ Mm}^{-1}$ at
346 450 nm and $0.24 (\pm 0.07) \text{ Mm}^{-1}$ at 660 nm according to the aethalometer, and $0.82 (\pm 0.13) \text{ Mm}^{-1}$ at
347 660 nm according to the MAAP. For the aethalometer, the absorption coefficient was calculated from

348 Eq. (2) assuming $C_{ref}=2.14$ and the R formulation by C2010 (Eq. 6b). The $\alpha(\lambda)$ coefficient was
349 calculated from Eq. (3). The c and d terms in Eq. (3) were determined from the power-law fit of $\beta_{ATT}(\lambda)$
350 vs $\beta_{sca}(\lambda)$ and are $c=(0.56 \pm 0.06) \text{ Mm}^{-1}$ and $d=(0.485 \pm 0.09)$. These values are lower than those
351 reported by Arnott et al. (2005) ($c=0.797$, $d=0.564$). The A and α_S terms, obtained from the power law
352 fit of $\beta_{sca}(\lambda)$ vs wavelength (Eq. 3) are $A=(4.07 \pm 0.49)10^9 \text{ Mm}^{-1}$ and $\alpha_S=(-2.46 \pm 0.12)$.

353 **Figure 4** shows the extinction coefficient at 660 nm extrapolated from CAPS observations and
354 calculated as the sum of nephelometer and MAAP data for dust, kaolinite, and ambient air
355 experiments. The linear regression of the data yields $y=1.03x-0.5$ ($R^2=0.99$), indicating the
356 consistency of optical measurements between the CAPS, nephelometer, and MAAP (less than 3%
357 difference on average). Based on the success of the optical closure at 660 nm, we therefore assume
358 the “CAPS minus nephelometer” approach appropriate to estimate the aerosol absorption coefficient
359 at 450 nm.

360 4.2. Estimate of C_{ref}

361 The C_{ref}^* , $C_{ref}(W2003)$ and $C_{ref}(C2010)$ at 450 and 660 nm obtained for all different experiments and
362 the corresponding aerosol SSA, $D_{eff, fine}$, and $D_{eff, coarse}$ are summarized in **Table 2**.

363 C_{ref} for mineral dust varied between 1.81 and 2.56 for a SSA of 0.85–0.96 at 450 nm and between
364 1.75 and 2.28 for a SSA of 0.98–0.99 at 660 nm. The estimate for Niger 1 and 2 samples agreed
365 within 4.9%, which suggests a good repeatability of the C_{ref} estimate. For kaolinite C_{ref} was 2.47–2.51
366 and 2.31–2.34 at 450 and 660 nm, respectively, with an associated SSA of 0.96 and 0.97 at the two
367 wavelengths. For ambient air C_{ref} varied in the range 1.91–4.35 for a SSA of 0.62–0.87 at 450 nm and
368 1.66–2.96 for and SSA of 0.42–0.76 at 660 nm. For samples 6 and 8 the C_{ref} at 450 was lower than at
369 660 nm. Otherwise, for all other cases, the C_{ref} was larger at 450 nm than at 660 nm.

370 Differences within 2.8% were obtained between C_{ref}^* , $C_{ref}(W2003)$ and $C_{ref}(C2010)$ at 450 and 660 nm
371 for weakly-absorbing dust and kaolinite. **Instead contrast**, for more absorbing ambient air aerosols the
372 differences between C_{ref}^* , $C_{ref}(W2003)$ and $C_{ref}(C2010)$ were in the range 2.7% to 24.3%. **The different**
373 **ATT threshold assumed here (20%) compared to W2003 and C2010 (10%) has a negligible impact**
374 **(less than 1% difference) on the results.**

375 In some cases (ambient air 1–2 and Niger 1 samples), **however**, we obtained
376 $C_{ref}(C2010)>C_{ref}(W2003)$; these cases correspond to a mean aethalometer measured ATT<10%, for
377 which $R(W2003)>R(C2010)$, and this explains the larger $C_{ref}(C2010)$. Conversely,
378 $C_{ref}(C2010)<C_{ref}(W2003)$ when the measured ATT was ~15-20%, yielding $R(W2003)<R(C2010)$. The
379 percent difference between the obtained $C_{ref}(W2003)$ and $C_{ref}(C2010)$ increased for decreasing SSA
380 due to the increase of the $R(W2003)$ to $R(C2010)$ absolute difference for decreasing SSA. When
381 averaging data for all ambient air samples, the two formulations yield very similar values. For
382 example, at 660 nm the mean $C_{ref}(W2003)$ was 2.44 (± 0.38), less than 2% larger than the mean
383 $C_{ref}(C2010)$ of 2.39 (± 0.35).

384 ~~The different ATT threshold assumed here (20%) compared to W2003 and C2010 (10%) has a~~
385 ~~negligible impact (less than 1% difference) on the results.~~

Mis en forme : Normal, Ne pas ajuster l'espace entre le texte latin et asiatique, Ne pas ajuster l'espace entre le texte et les nombres asiatiques

386 The mean and standard deviation of the multiple scattering correction at 450 and 660 nm for dust,
387 kaolinite, and ambient air calculated as the mean of the C_{ref}^* , $C_{ref}(W2003)$, and $C_{ref}(C2010)$ ~~are~~
388 reported in **Table 3**. The mean C_{ref} at 450 and 660 nm is 2.09 (± 0.22) and 1.92 (± 0.17) for dust, 2.49
389 (± 0.02) and 2.31~~2~~ (± 0.04)~~2~~ for kaolinite, and 2.32 (± 0.36) and 2.32 (± 0.35) for pollution aerosols. If
390 the wavelength of 637 nm is assumed for the MAAP instead of 670 nm, as suggested by Müller et al.
391 (2011), the average C_{ref} at 660 nm would increase by up to ~15% for dust and ambient air (2.17 \pm 0.19
392 and 2.48 \pm 0.41, respectively) and ~3% for kaolinite (2.40 \pm 0.02).

393 4.3. Dependence of C_{ref} on SSA

394 As reported in Table 2, very different SSA values at 450 and 660 nm were obtained for the various
395 cases. For dust aerosols, the measured SSA values were larger than 0.85 at 450 nm and close to
396 unity (>0.98) at 660 nm, in line with field observations of dust from different sources (Schladitz et al.,
397 2009; Formenti et al., 2011; Ryder et al., 2013). In particular, our results for China, Arizona, and
398 Australia samples are in line with published values by Engelbrecht et al. (2016), who used a
399 photoacoustic instrument to measure absorption of re-suspended dust aerosols. This would suggest
400 the similar performances of the aethalometer compared to the photoacoustic technique. The SSA for
401 kaolinite was 0.96–0.97 at 450 and 660 nm, in agreement with Utry et al. (2017~~6~~) also using a
402 photoacoustic method to measure absorption (0.97 and 0.99 (± 0.04)) at 450 and 635 nm, respectively).
403 Both at 450 and 660 nm, the single scattering albedo for ambient air varied in the wide range 0.2 to
404 0.9 during the whole measurement period (see Fig. 2 for measurements at 660 nm). The average
405 values obtained for air samples 1–8 were 0.62–0.87 at 450 and 0.42–0.76 at 660 nm. The SSA
406 decreased with increasing wavelength, as expected for pollution aerosols (e.g., Bergstrom et al.,
407 2007; Di Biagio et al., 2016). The wide range of values indicates the occurrence of particles with very
408 different absorption properties, henceforth chemical composition (or complex refractive index) and/or
409 different size distribution (e.g., Moosmüller and Arnott, 2009). For instance, in urban environments,
410 Bergstrom et al. (2007) reported SSA in the range 0.2–1.0 at 550 nm, with lowest values observed for
411 soot-dominated air masses and highest values for urban pollution dominated by low-absorbing
412 organic components.

413 The experimental SSA values served ~~to~~ two purposes. First, as shown in **Fig. 5**, they are linearly
414 related to the factor f in the ~~shadowing-loading~~ effect correction term R in Eq. (6a)-(6b) as $f = a(1 -$
415 $SSA) + 1$. The linear regression of our data yields a slope $a = (1.48 \pm 0.14)$, larger than the value of 0.85
416 reported in W2003 (f data from W2003 are also shown in Fig. 5) and 0.76 in C2010.

417 Secondly, SSA data serve to investigate the dependence of C_{ref} on relative amounts of particle
418 absorption for mineral dust. As shown in **Fig. 6** (top panel), C_{ref} for dust seems to be independent of
419 SSA at 660 nm, whereas it decreases for increasing SSA at 450 nm. This trend is statistically
420 significant (correlation coefficient of $R^2 = 0.85$). The relationship between C_{ref} and SSA is also
421 investigated in **Fig. 6** (bottom panel) for all aerosol samples. Globally, Fig. 6 suggests a decrease of
422 C_{ref} for increasing SSA, in particular at 450 nm, albeit with a poorer statistical significance at both
423 wavelengths ($R^2 = 0.35$ and 0.59). Data are also compared to those reported in W2003 and C2010 at
424 660 nm for different aerosol types. Diesel soot and soot mixed with ammonium sulfate were

Mis en forme : Police :10 pt, Non Surlignage

Mis en forme : Police :10 pt, Non Surlignage

425 investigated in W2003, while C2010 reported data for ambient aerosols sampled at different locations
426 in Europe and in Amazonia. W2003 also reported the C_{ref} for soot particles at 450 nm (not shown in
427 Fig. 6), with values between 2.08 and 3.64; these values are in line with our observations at 450 nm
428 for ambient air. Whereas, as illustrated in Fig. 6, both W2003 and C2010 found a relationship
429 between C_{ref} and SSA at 660 nm, contrasting results are obtained when plotting the two datasets
430 together. C2010 obtained a sharp and almost linear decrease of C_{ref} with increasing SSA ($C_{ref} \sim 5-2.5$
431 for $SSA \sim 0.65-0.9$), while W2003 data showed a pronounced decrease of C_{ref} ($\sim 2-4$) for increasing
432 SSA in the range 0.5 and 0.7 and low C_{ref} values (~ 2) at $SSA \sim 0.2$. Our data for dust and kaolinite at
433 high SSA (>0.97) seem to follow the same linear relationship as C2010. However at lower SSA, our
434 data for ambient aerosols are closer to W2003 results at 660 nm. These differences between W2003
435 and C2010 data, and also with our results, are quite difficult to explain. The main difference between
436 W2003 compared to C2010 is that W2003 performed measurements in a simulation chamber, while
437 C2010 was a field study. Working in ambient conditions may influence the retrieved C_{ref} . In fact,
438 volatile-organic compounds or water vapor present in the atmosphere may condense on the filter
439 ([Lack et al., 2008](#)), thus enhancing the scattering from the filter fibers and leading to higher C_{ref} . This
440 could explain the higher C_{ref} obtained in C2010 compared to W2003. Our results for ambient air
441 particles, however, are in agreement with W2003 chamber results. Differences in the size distributions
442 of the investigated aerosols are also expected to possibly affect the comparison; however, no detailed
443 information on the size of investigated aerosols is provided in W2003 and C2010. Another source of
444 discrepancy may be in the fact that, differently from W2003 and our study, where aethalometer and
445 MAAP were compared at 660 nm, C_{ref} in C2010 was estimated by comparing aethalometer data at
446 660 nm with MAAP observations at 630 nm. As aerosol absorption increases with decreasing
447 wavelength, this wavelength difference may induce an underestimation of C_{ref} in C2010.

448 **4.4. Dependence of C_{ref} on particles size**

449 Examples of the number size distribution measured by the SMPS and OPC for ammonium sulfate,
450 Niger dust, kaolinite, and ambient air are shown in **Fig. 7**. Ammonium sulfate had mostly a submicron
451 distribution, while dust aerosols presented the largest fraction over the whole super-micron range up
452 to about 10-20 μm . Dust particles larger than 20 μm were completely suppressed by the impactor
453 system and were not detected by the OPC. The coarse component, up to about 10 μm , was also
454 identified in the kaolinite and ambient air samples. In particular, a defined mode at $\sim 4 \mu\text{m}$ was
455 detected in [the number distribution of](#) ambient air particles, [and](#) may be linked to the presence of
456 soot-aggregates, tire abrasions, re-suspended road dust, or bioaerosols (Harrison et al., 2001; Bauer
457 et al., 2008; Pakbin et al., 2010; Liu and Harrison, 2011). ~~In correspondence,~~ The $D_{eff, fine}$ varied
458 between 0.24 and 0.62 μm and the $D_{eff, coarse}$ between 2.3 and 6.2 μm for the different cases (Table 2).
459 For mineral dust, $D_{eff, coarse}$ ranged between 2.3 and 3.6 μm , encompassing the value of $D_{eff, coarse} \sim 3$
460 μm reported by Denjean et al. (2016b) in their figure 11 for Saharan dust both close to sources and
461 during transport over the Atlantic.

462 These observations are consistent with the extinction (α_E) and the absorption (α_A) Ångstrom exponent
463 measured during the experiments. The α_E (shown in [Fig. 32](#)) was $\sim 1-0$ for kaolinite, varied between

464 | about 0.4 and 2 for mineral dust aerosols, and between 0.5 and 2.5 for ambient air, indicating particles
465 | with variable sizes, both the sub-micron and the super-micron fractions. The absorption Ångström
466 | coefficient α_A obtained from aethalometer data was between 2.2 and 3.4 for dust, between 1 and
467 | 1.5 and about 4 for kaolinite and between 0.5 and 1.5 for ambient air aerosols.

Mis en forme : Non Surlignage

Mis en forme : Non Surlignage

468 | The dependence of C_{ref} at 450 and 660 nm on the effective diameter fine $D_{eff, fine}$ and coarse $D_{eff, coarse}$
469 | as a measure of particle size was investigated. The scatterplot of C_{ref} versus $D_{eff, coarse}$ is shown in Fig.
470 | 8 and indicates that the C_{ref} does not have any statistically significant dependence on the particle size
471 | for mineral dust at both wavelengths and for all data at 660 nm ($R^2 \leq 0.40$). Conversely, a slight
472 | increase of C_{ref} for increasing $D_{eff, coarse}$ is obtained at 450 nm when all aerosol samples are considered
473 | ($R^2 = 0.70$). In contrast, No dependence of C_{ref} versus on $D_{eff, fine}$ is instead obtained found for all cases
474 | ($R^2 \leq 0.44$) (not shown).

475

476 | 5. Conclusions

477 | In this paper we presented an intercomparison study between an aethalometer and a MAAP, a
478 | nephelometer, and two CAPS with the aim of determining a two-wavelength multiple scattering
479 | correction (C_{ref}) for aethalometer measurements for weakly-absorbing mineral dust aerosols. Mineral
480 | dust aerosols investigated here were generated from natural parent soils collected in desert areas,
481 | both in the Northern and in the Southern hemisphere (Di Biagio et al., 2014; 2017). The size
482 | distribution of the generated dust included both the submicron and the supermicron fractions, with an
483 | effective fine and coarse diameter between 0.32–0.55 and 2.3–3.6 μm , respectively.

484 | The estimated C_{ref} was in the range 1.81–2.56 at 450 nm and 1.75–2.28 at 660 nm for the different
485 | dust samples, with mean C_{ref} values of 2.09 (± 0.22) and 1.92 (± 0.17), respectively. Using these
486 | values of C_{ref} , The dust absorption coefficient estimated by the aethalometer should henceforth will be
487 | about 2% (450 nm) and 11% (660 nm) higher than obtained by using the wavelength-independent
488 | value of 2.14, commonly used in the literature (e.g., Sandradewi et al., 2008; Formenti et al., 2011; Di
489 | Biagio 2016). The new estimate of C_{ref} has a negligible impact on the dust SSA at 450 nm (less than
490 | 0.5% difference between the value obtained for $C_{ref} = 2.09$ or 2.14), but affects by up to ~3% the
491 | estimate of SSA at 660 nm.

492 | Given that the median maximum intensity of the solar spectrum occurs at about 700 nm, the expected
493 | change in the dust SSA at 660 nm may significantly affect the impact of dust on radiation. Mallet et al.
494 | (2009) estimated that about a 3% change in the visible SSA of dust may determine up to a 10%
495 | change in the radiative effect of dust at the surface, and up to 20% change at the Top of the
496 | Atmosphere, with a net ~25% increase of dust absorption in the atmosphere. Given the strong
497 | sensitivity of the dust direct effect to particle absorption (Solmon et al., 2008; Mallet et al., 2009; Di
498 | Biagio et al., 2010; Jin et al., 2016, among others), we recommend this new C_{ref} value at 660 nm to be
499 | used when analyzing aethalometer data for mineral dust aerosols.

500 | The analysis performed in this study indicates that there is no dependence of C_{ref} on the coarse
501 | component of the particle size distribution for dust. This suggests that the C_{ref} obtained here can be

502 used to correct aethalometer data for dust at emission, when the coarse fraction dominates the dust
503 size distribution, as well as after long-range transport, when the coarsest component of dust has
504 preferentially settled out.

505 Finally, ~~even if beyond the scope of the paper,~~ our body of observations, spanning a wide range of
506 SSA values from 0.96–0.97 (kaolinite) to ~0.4–0.8 (ambient urban aerosols), indicates that C_{ref}
507 decreases for increasing SSA, both at 450 and 660 nm. This is generally consistent with the results of
508 W2003 and C2010 at 660 nm. However, a unique relationship cannot be established. At high SSA
509 (>0.90), our data, as well as those of C2010, suggest a sharper decrease than at SSA in the range
510 0.4–0.8, where our data are more consistent with those of W2003. Differences in aerosol sampling
511 conditions and in the exact analysed wavelengths from the three studies may be the cause of such
512 discrepancy, but clear conclusions, as well as an explicit relationship between C_{ref} and SSA, are still
513 difficult to give. Similarly, our observations seem to indicate that C_{ref} increases for increasing $D_{eff,coarse}$
514 at 450 nm. This trend was ~~however only~~ observed ~~only~~ when the ~~whole aerosol entire~~ dataset was
515 considered, ~~and but~~ not if the dataset was limited to just the dust observations, ~~so~~ making it difficult
516 to draw clear conclusions.

517 A more extensive characterization of C_{ref} ~~should be is~~ required to provide an appropriate correction of
518 aethalometer data under the wide range of atmospheric conditions.

519

520 Author contributions

521 C. Di Biagio and P. Formenti designed the experiments, discussed the results, and wrote the
522 manuscript with comments from all co-authors. N. Marchand provided the MAAP used in the
523 experiments. C. Di Biagio, M. Cazaunau, and E. Pangui performed the experiments. C. Di Biagio
524 performed the data analysis.

525

526 Acknowledgements

527 The RED-DUST project was supported by the French national programme LEFE/INSU, by the Institut
528 Pierre Simon Laplace (IPSL), and by OSU-EFLUVE (Observatoire des Sciences de l'Univers-
529 Enveloppes Fluides de la Ville à l'Exobiologie) through dedicated research funding. C. Di Biagio was
530 supported by the CNRS via the Labex L-IPSL, which is funded by the ANR (grant no. ANR-10-LABX-
531 0018). This work has also received funding from the European Union's Horizon 2020 (H2020)
532 research and innovation programme through the EUROCHAMP-2020 Infrastructure Activity under
533 grant agreement No 730997. The authors thank K. Kandler, D. Seibert, and the LISA staff who
534 collected the soil samples used in this study, E. Journet who provided the kaolinite sample, A. Petzold
535 for helpful discussions on the aethalometer multiple scattering effects, and B. Tamime-Roussel for
536 logistic help with the MAAP.

537

538 References

- 539 Anderson, T. L. and Ogren, J. A.: Determining aerosol radiative properties using the TSI 3563
540 integrating nephelometer, *Aerosol Sci. Technol.*, 29, 57–69, 1998.
- 541 Andreae, M. O. and Gelencsér, A.: Black Carbon or Brown Carbon? The Nature of Light-Absorbing
542 Carbonaceous Aerosols. *Atmos. Chem. Phys.* 6:3131–3148, 2006.
- 543 Arnott, W. P., Hamasha, K., Moosmüller, H., Sheridan, P. J., and Ogren, J. A.: Towards aerosol
544 light-absorption measurements with a 7-wavelength aethalometer: Evaluation with a photoacoustic
545 instrument and 3-wavelength nephelometer, *Aerosol Sci. Tech.*, 39, 17–29, 2005.
- 546 Backman, J., Schmeisser, L., Virkkula, A., Ogren, J. A., Asmi, E., Starkweather, S., Sharma, S.,
547 Eleftheriadis, K., Uttal, T., Jefferson, A., Bergin, M., and Makshtas, A.: On Aethalometer
548 measurement uncertainties and multiple scattering enhancement in the Arctic, *Atmos. Meas. Tech.*
549 *Discuss.*, doi:10.5194/amt-2016-294, in review, 2016.
- 550 Balkanski, Y., Schulz, M., Claquin, T., and Guibert, S.: Reevaluation of Mineral aerosol radiative
551 forcings suggests a better agreement with satellite and AERONET data, *Atmos. Chem. Phys.*, 7,
552 81–95, doi:10.5194/acp-7-81-2007, 2007.
- 553 Bauer, H., Schueller, E., Weinke, G., Berger, A., Hitznerberger, R., Marr, I. L., and Puxbaum, H.:
554 Significant contributions of fungal spores to the organic carbon and to the aerosol mass balance of
555 the urban atmospheric aerosol, *Atmos. Environ.*, 42, 5542-5549, 2008.
- 556 Bergstrom, R. W., Pilewskie, P., Russell, P. B., Redemann, J., Bond, T. C., Quinn, P. K., and Sierau,
557 B.: Spectral absorption properties of atmospheric aerosols, *Atmos. Chem. Phys.*, 7, 5937-5943,
558 doi:10.5194/acp-7-5937-2007, 2007.
- ~~559 Bond, T. C., Anderson, T. L., and Campbell, D.: Calibration and intercomparison of filter-based
560 measurements of visible light absorption by aerosols, *Aerosol Sci. Tech.*, 30(6), 582–600, 1999.~~
- ~~561 Boucher, O., Randall, D., Artaxo, P., Bretherton, C., Feingold, G., Forster, P., Kerminen, V. M.,
562 Kondo, Y., Liao, H., Lohmann, U., Rasch, P., Sathesh, S. K., Sherwood, S., Stevens, B., and
563 Zhang, X. Y.: Clouds and Aerosols. In: *Climate Change 2013: The Physical Science Basis.*
564 *Contribution of Working Group I to the Fifth Assessment Report of the Intergovernmental Panel on*
565 *Climate Change* [Stocker, T.F., D. Qin, G. K. Plattner, M. Tignor, S.K. Allen, J. Boschung, A. Nauels,
566 Y. Xia, V. Bex and P.M. Midgley (eds.)]. Cambridge University Press, Cambridge, United Kingdom
567 and New York, NY, USA, 2013.~~
- 568 Caponi, L., Formenti, P., Massabó, D., Di Biagio, C., Cazaunau, M., Pangui, E., Chavaille, S.,
569 Landrot, G., Fonda, E., Andreae, M. O., Kandler, K., Piketh, S., Saeed, T., Seibert, D., Williams, E.,
570 Balkanski, Y., Prati, P., and Doussin, J.-F.: Spectral- and size-resolved shortwave mass absorption
571 cross-sections of mineral dust aerosols: a smog chamber study, *Atmos. Chem. Phys.*, 17, 7175-
572 7191, <https://doi.org/10.5194/acp-17-7175-2017>, 2017 *Atmos. Chem. Phys. Discuss.*,
573 doi:10.5194/acp-2017-5, in review, 2017.
- 574 Cattrall, C., Carder, K. L., and Gordon, H. R.: Columnar aerosol single-scattering albedo and phase
575 function retrieved from sky radiance over the ocean: measurements of Saharan dust, *J. Geophys.*
576 *Res.*, 108(D9), 4287, doi:10.1029/2002JD002497, 2003.
- 577 Collaud Coen, M., Weingartner, E., Apituley, A., Ceburnis, D., Fierz-Schmidhauser, R., Flentje, H.,
578 Henzing, J. S., Jennings, S. G., Moerman, M., Petzold, A., Schmid, O., and Baltensperger, U.:
579 Minimizing light absorption measurement artifacts of the Aethalometer: evaluation of five correction
580 algorithms, *Atmos. Meas. Tech.*, 3, 457–474, doi:10.5194/amt-3-457-2010, 2010.
- 581 DeCarlo, P., Worsnop, D. R., Slowik, J. G., Davidovits, P., and Jimenez, J. L.: Particle Morphology
582 and Density Characterization by Combined Mobility and Aerodynamic Diameter Measurements. Part
583 1: Theory, *Aerosol Sci. Technol.*, 38(12), 1185-1205, 2004.
- 584 Denjean, C., Formenti, P., Desboeufs, K., Chevaillier, S., Triquet, S., Maillé, M., Cazaunau, M.,
585 Laurent, B., Mayol-Bracero, O. L., Vallejo, P., Quiñones, M., Gutierrez-Molina, I. E., Cassola, F.,
586 Prati, P., Andrews, E., and Ogren, J.: Size distribution and optical properties of African mineral dust
587 after intercontinental transport, *J. Geophys. Res. Atmos.*, 121, 7117–7138,
588 doi:10.1002/2016JD024783, 2016a.
- 589 Denjean, C., Cassola, F., Mazzino, A., Triquet, S., Chevaillier, S., Grand, N., Bourriane, T.,
590 Momboisse, G., Sellegri, K., Schwarzenbock, A., Freney, E., Mallet, M., and Formenti, P.: Size

Mis en forme : Police :(Par défaut)
Arial, 10 pt

Mis en forme : Police :Non Italique

Mis en forme : Police :(Par défaut)
Arial, 10 pt

- 591 distribution and optical properties of mineral dust aerosols transported in the western Mediterranean,
592 Atmos. Chem. Phys., 16, 1081-1104, doi:10.5194/acp-16-1081-2016, 2016b.
- 593 Di Biagio, C., di Sarra, A., and Meloni, D.: Large atmospheric shortwave radiative forcing by
594 Mediterranean aerosols derived from simultaneous ground-based and spaceborne observations and
595 dependence on the aerosol type and single scattering albedo, J. Geophys. Res., 115, D10209, doi:
596 10.1029/2009JD012697, 2010.
- 597 Di Biagio, C., Formenti, P., Styler, S. A., Pangui, E., and Doussin, J.-F.: Laboratory chamber
598 measurements of the longwave extinction spectra and complex refractive indices of African and
599 Asian mineral dusts, Geophys. Res. Lett., 41, 6289-6297, doi:10.1002/2014GL060213, 2014.
- 600 Di Biagio, C., Formenti, P., Doppler, L., Gaimoz, C., Grand, N., Ancellet, G., Attié, J.-L., Bucci, S.,
601 Dubuisson, P., Fierli, F., Mallet, M., and Ravetta, F.: Continental pollution in the Western
602 Mediterranean basin: large variability of the aerosol single scattering albedo and influence on the
603 direct shortwave radiative effect, Atmos. Chem. Phys., 16, 10591-10607, doi:10.5194/acp-16-10591-
604 2016, 2016.
- 605 Di Biagio, C., Formenti, P., Balkanski, Y., Caponi, L., Cazaunau, M., Pangui, E., Journet, E., Nowak,
606 S., Caquineau, S., Andreae, M. O., Kandler, K., Saeed, T., Piketh, S., Seibert, D., Williams, E., and
607 Doussin, J.-F.: Global scale variability of the mineral dust longwave refractive index: a new dataset
608 of in situ measurements for climate modelling and remote sensing, Atmos. Chem. Phys., 17, 1901-
609 1929, doi:10.5194/acp-17-1901-2017, 2017.
- 610 di Sarra, A., C. Di Biagio, D. Meloni, F. Monteleone, G. Pace, S. Pugnaghi, and D. Sferlazzo,
611 Shortwave and longwave radiative effects of the intense Saharan dust event of March 25-26, 2010,
612 at Lampedusa (Mediterranean sea), J. Geophys. Res., 116, D23209, doi:10.1029/2011JD016238,
613 2011.
- 614 Egan, W. G. and Hilgeman, T. W.: Optical Properties of Inhomogeneous Materials: Applications to
615 Geology, Astronomy, Chemistry, and Engineering, Academic Press, 235 pp, 1979.
- 616
- 617 Engelbrecht, J. P., Moosmüller, H., Pincock, S., Jayanty, R. K. M., Lersch, T., and Casuccio, G.:
618 Technical note: Mineralogical, chemical, morphological, and optical interrelationships of mineral dust
619 re-suspensions, Atmos. Chem. Phys., 16, 10809-10830, doi:10.5194/acp-16-10809-2016, 2016.
- 620 Fialho, P., Hansen, A. D. A., and Honrath, R. E.: Absorption coefficients by aerosols in remote
621 areas: a new approach to decouple dust and black carbon absorption coefficients using seven-
622 wavelength Aethalometer data, Aerosol Sci., 36, 267-282, 2005.
- 623 Formenti, P., Rajot, J. L., Desboeufs, K., Said, F., Grand, N., Chevaillier, S., and Schmechtig, C.:
624 Airborne observations of mineral dust over western Africa in the summer Monsoon season: spatial
625 and vertical variability of physico-chemical and optical properties, Atmos. Chem. Phys., 11, 6387-
626 6410, doi:10.5194/acp-11-6387-2011, 2011.
- 627 ~~Ginoux, P., Prospero, J. M., Gill, T. E., Hsu, N. C., and Zhao, M.: Global scale attribution of~~
628 ~~anthropogenic and natural dust sources and their emission rates based on MODIS Deep Blue~~
629 ~~aerosol products, Rev. Geophys., 50, RG3006, doi:10.1029/2012RG000388, 2012.~~
- 630 Goudie A. S., and Middleton, N. J.: Desert dust in the global system. Springer, Berlin, Heidelberg,
631 New York, 2006.
- 632 Hansen, A. D. A., Rosen, H., and Novakov, T.: The aethalometer—an instrument for the real-time
633 measurement of optical absorption by aerosol particles. The Science of the Total Environment, 36,
634 191-196, 1984.
- 635 Harrison, R. M., Yin, J., Mark, D., Stedman, J., Appleby, R.S., Booker, J., and Moorcroft, S.: Studies
636 of the coarse particle (2.5–10 µm) component in UK urban atmospheres, Atmos. Environ., 35,
637 3667-3679, 2001.
- 638 Heim, M., Mullins, B. J., Umhauer, H., and Kasper, G.: Performance evaluation of three optical
639 particle counters with an efficient “multimodal” calibration method, J. Aerosol Sci., 39, 1019-1031,
640 2008.
- 641

Mis en forme : Police :(Par défaut)
Arial, 10 pt

Mis en forme : Couleur de police :
Automatique

Mis en forme : Retrait : Gauche : 0
cm, Suspendu : 0.25 cm, Espace Avant
: 6 pt, Interligne : simple, Autoriser
lignes veuves et orphelines, Ne pas
ajuster l'espace entre le texte latin et
asiatique, Ne pas ajuster l'espace entre
le texte et les nombres asiatiques

- 692 Weingartner, E., Wilhelm, R., and Wang, Y. Q.: Characterization and intercomparison of aerosol
693 absorption photometers: result of two intercomparison workshops, *Atmos. Meas. Tech.*, 4, 245-268,
694 doi:10.5194/amt-4-245-2011, 2011.
- 695 Pakbin, P., Hudda, N., Cheng, K. L., Moore, K. F., Sioutas, C.: Spatial and temporal variability of
696 coarse (PM_{10-2.5}) particulate matter concentrations in the Los Angeles area, *Aerosol Sci. Technol.*,
697 44, 514–525, 2010.
- 698 Perez, C., Nickovic, S., Baldasano, J. M., Sicard, M., Rocadenbosch, F., and Cachorro, V. E.: A long
699 Saharan dust event over the western Mediterranean: Lidar, Sun photometer observations, and
700 regional dust modeling, *J. Geophys. Res.*, 111, D15214, doi:10.1029/2005JD006579, 2006.
- 701
- 702 Petzold, A., and Schönlinner, M.: Multiangle Absorption Photometry—A New Method for the
703 Measurement of Aerosol Light Absorption and Atmospheric Black Carbon, *J. Aerosol Sci.*, 35:421–
704 441, 2004.
- 705 Petzold, A., Schloesser, H., Sheridan, P. J., Arnott, W. P., Ogren, J. A., and Virkkula, A.: Evaluation of
706 Multi-angle Absorption Photometry for Measuring Aerosol Light Absorption, *Aerosol Sci. Technol.*,
707 39, 40–51, 2005.
- 708 Querol, X., Pey, J., Pandolfi, M., Alastuey, A., Cusack, M., Pérez, N., Moreno, T., Viana, M.,
709 Mihalopoulos, N., Kallos, G., and Kleanthous, S.: African dust contributions to mean ambient PM10
710 mass-levels across the Mediterranean Basin, *Atmos. Environ.*, 43, 4266-4277, 2009.
- 711 ~~Ramana, M. V., and Ramanathan, V.: Abrupt transition from natural to anthropogenic aerosol
712 radiative forcing: Observation at the ABCMaldives Climate Observatory, *J. Geophys. Res.*, 111,
713 D20207, doi:10.1029/2006JD007063, 2006.~~
- 714 Reddy, M. S., O. Boucher, Y. Balkanski, and M. Schulz: Aerosol optical depths and direct radiative
715 perturbations by species and source type. *Geophys. Res. Lett.*, 32, L12803, 2005.
- 716 Redmond, H. E., Dial, K. D., and Thompson, J. E.: Light scattering and absorption by wind blown
717 dust: Theory, measurement, and recent data, *Aeolian Res.*, 2, 5–26, 2010.
- 718 Ryder, C. L., Highwood, E. J., Rosenberg, P. D., Trembath, J., Brooke, J. K., Bart, M., Dean, A.,
719 Crosier, J., Dorsey, J., Brindley, H., Banks, J., Marsham, J. H., McQuaid, J. B., Sodemann, H., and
720 Washington, R.: Optical properties of Saharan dust aerosol and contribution from the coarse mode
721 as measured during the Fennec 2011 aircraft campaign, *Atmos. Chem. Phys.*, 13, 303-325,
722 doi:10.5194/acp-13-303-2013, 2013.
- 723 Sandradewi, J., Prévôt, A. S. H., Weingartner, E., Schmidhauser, R., Gysel, M., and Baltensperger,
724 U.: A study of wood burning and traffic aerosols in an Alpine valley using a multi-wavelength
725 Aethalometer, *Atmos. Environ.*, 42, 101-112, 2008.
- 726 Saturno, J., Pöhlker, C., Massabò, D., Brito, J., Carbone, S., Cheng, Y., Chi, X., Ditas, F., Hrabě de
727 Angelis, I., Morán-Zuloaga, D., Pöhlker, M. L., Rizzo, L. V., Walter, D., Wang, Q., Artaxo, P., Prati,
728 P., and Andreae, M. O.: Comparison of different Aethalometer correction schemes and a reference
729 multi-wavelength absorption technique for ambient aerosol data, *Atmos. Meas. Tech. Discuss.*,
730 doi:10.5194/amt-2016-361, in review, 2016.
- 731 Schladitz, A., Müller, T., Kaaden, N., Massling, A., Kandler, K., Ebert, M., Weinbruch, S., Deutscher,
732 C., and Wiedensohler, A.: In situ measurements of optical properties at Tinfou (Morocco) during the
733 Saharan Mineral Dust Experiment SAMUM 2006, *Tellus B*, 61, 64–78, doi:10.1111/j.1600-
734 0889.2008.00397.x, 2009.
- 735 Schmid, O., Artaxo, P., Arnott, W. P., Chand, D., Gatti, L. V., Frank, G. P., Hoffer, A., Schnaiter, M.,
736 and Andreae, M. O.: Spectral light absorption by ambient aerosols influenced by biomass burning in
737 the Amazon Basin. I: Comparison and field calibration of absorption measurement techniques,
738 *Atmos. Chem. Phys.*, 6, 3443–3462, 2006.
- 739 Segura, S., Estellés, V., Titos, G., Lyamani, H., Utrillas, M. P., Zotter, P., Prévôt, A. S. H., Močnik, G.,
740 Alados-Arboledas, L., and Martínez-Lozano, J. A.: Determination and analysis of in situ spectral
741 aerosol optical properties by a multi-instrumental approach, *Atmos. Meas. Tech.*, 7, 2373-2387, doi:
742 10.5194/amt-7-2373-2014, 2014.

Mis en forme : Retrait : Gauche : 0
cm, Suspendu : 0.25 cm

Mis en forme : Retrait : Gauche : 0
cm, Suspendu : 0.25 cm

Mis en forme : Non souligné, Couleur
de police : Automatique

743 [Sherman, J. P., Sheridan, P. J., Ogren, J. A., Andrews, E., Hageman, D., Schmeisser, L., Jefferson,](#)
744 [A., and Sharma, S.: A multi-year study of lower tropospheric aerosol variability and systematic](#)
745 [relationships from four North American regions, Atmos. Chem. Phys., 15, 12487-12517,](#)
746 [doi:10.5194/acp-15-12487-2015, 2015.](#)

747 Slingo, A., et al., Observations of the impact of a major Saharan dust storm on the atmospheric
748 radiation balance, Geophys. Res. Lett., 33, L24817, doi:10.1029/2006GL027869, 2006.

749 Sokolik, I., and Toon, O.: Incorporation of mineralogical composition into models of the radiative
750 properties of mineral aerosol from UV to IR wavelengths, J. Geophys. Res., 104, 9423-9444, 1999.

751 Solmon, F., Mallet, M., Elguindi, N., Giorgi, F., Zakey, A. and Konaré, A.: Dust aerosol impact on
752 regional precipitation over western Africa, mechanisms and sensitivity to absorption properties,
753 Geophys. Res. Lett., 35, L24705, doi:10.1029/2008GL035900, 2008.

754 Toon, O. B., Pollack, J. B., and Khare, B. N.: The Optical Constants of Several Atmospheric Aerosol
755 Species: Ammonium Sulfate, Aluminum Oxide, and Sodium Chloride, J. Geophys. Res., 81, 5733–
756 5748, 1976.

757 Utry, N., Ajtai, T., Pintér, M., Tombácz, E., Illés, E., Bozóki, Z., and Szabó, G.: Mass-specific optical
758 absorption coefficients and imaginary part of the complex refractive indices of mineral dust
759 components measured by a multi-wavelength photoacoustic spectrometer, Atmos. Meas. Tech., 8,
760 401-410, doi:10.5194/amt-8-401-2015, 2015.

761 [Utry, N., Ajtai, T., Pintér, M., Illés, E., Tombácz, E., Szabó, G., and Bozóki, Z.: Generation and UV-](#)
762 [VIS-NIR spectral responses of organo-mineral aerosol for modelling soil derived dust, Atmos.](#)
763 [Environ., 152, 553-561, 2017.,](#)

764 Virkkula, A., Makela, T., Hillamo, R., Yli-Tuomi, T., Hirsikko, A., Hameri, K., and Koponen, I. K.: A
765 simple procedure for correcting loading effects of aethalometer data, J. Air Waste Manage., 57(10),
766 1214–1222, 2007.

767 von der Weiden, S.-L., Drewnick, F., and Borrmann, S.: Particle Loss Calculator – a new software tool
768 for the assessment of the performance of aerosol inlet systems, Atmos. Meas. Tech., 2, 479–494,
769 2009.

770 Weingartner, E., Saathof, H., Schnaiter, M., Streit, N., Bitnar, B., and Baltensperger, U.: Absorption of
771 light by soot particles: Determination of the absorption coefficient by means of Aethalometers, J.
772 Aerosol Sci., 34, 1445–1463, 2003.

773 Yoshioka, M., N.M.Mahowald, A. J. Conley, W. D. Collins, D.W. Fillmore, C. S. Zender, and D. B.
774 Coleman: Impact of desert dust radiative forcing on sahel precipitation: Relative importance of dust
775 compared to sea surface temperature variations, vegetation changes, and greenhouse gas
776 warming, J. Clim., 20, 1445– 1467, 2007.
777

Mis en forme : Non Surlignage

Mis en forme : Police :(Par défaut)
Arial, 10 pt

Mis en forme : Police :(Par défaut)
Arial, 10 pt

Mis en forme : Police :(Par défaut)
Arial, 10 pt

Mis en forme : Police :(Par défaut)
Arial, 10 pt, Non Italique

Mis en forme : Police :(Par défaut)
Arial, 10 pt

Mis en forme : Police :(Par défaut)
Arial, 10 pt, Non Italique

Mis en forme : Police :(Par défaut)
Arial, 10 pt

Mis en forme : Police :(Par défaut)
Arial, 10 pt, Non Italique

Mis en forme : Police :(Par défaut)
Arial, 10 pt

Mis en forme : Surlignage

Mis en forme : Justifié, Retrait :
Gauche : 0 cm, Suspendu : 0.25 cm,
Espace Avant : 6 pt, Après : 0 pt,
Interligne : simple, Ne pas ajuster
l'espace entre le texte latin et asiatique,
Ne pas ajuster l'espace entre le texte et
les nombres asiatiques

778 **Table captions**

779 **Table 1.** Specifications and references of instruments used during experiments.

780 **Table 2.** Summary of experiments and results. The mean and the standard deviation of $D_{\text{eff, fine}}$,
781 $D_{\text{eff, coarse}}$, SSA at 450 and 660 nm, C_{ref}^* , $C_{\text{ref}}(\text{W2003})$, and $C_{\text{ref}}(\text{C2010})$ are reported. As a reminder:
782 C_{ref}^* is the multiple scattering correction obtained not taking into account the shadowing-loading effect
783 correction in aethalometer data; $C_{\text{ref}}(\text{W2003})$ and $C_{\text{ref}}(\text{C2010})$ take the shadowing-loading effect
784 correction into account, by using the parametrisations by Weingartner et al. (2003) (referred as
785 W2003) and Collaud Coen et al. (2010) (referred as C2010), respectively. The maximum of the %
786 difference between C_{ref}^* , $C_{\text{ref}}(\text{W2003})$, and $C_{\text{ref}}(\text{C2010})$ is indicated in the table.

787 **Table 3.** Mean and standard deviation multiple scattering correction $\overline{C_{\text{ref}}}$ at 450 and 660 nm for dust,
788 kaolinite, and ambient air. The $\overline{C_{\text{ref}}}$ was calculated as the mean of the C_{ref}^* , $C_{\text{ref}}(\text{W2003})$, and
789 $C_{\text{ref}}(\text{C2010})$ obtained at each wavelength for the different aerosol types. As a reminder: C_{ref}^* is the
790 multiple scattering correction obtained not taking into account the shadowing-loading effect correction
791 in aethalometer data; $C_{\text{ref}}(\text{W2003})$ and $C_{\text{ref}}(\text{C2010})$ take the shadowing-loading effect correction into
792 account, by using the parametrisations by Weingartner et al. (2003) and Collaud Coen et al. (2010),
793 respectively.

794

795 **Figure captions**

796 **Figure 1.** Experimental setup used for the aethalometer intercomparison experiments.

797 **Figure 2.** Temporal series of experiments showing the measured optical data at 660 nm. The different
798 panels show (from the top to the bottom): (i) the shadowingloading-corrected aethalometer
799 attenuation at 660 nm (data corrected with the R formulation by Collaud Coen et al. (2010) (referred
800 to as R(C2010)) are shown) and the MAAP aerosol absorption coefficient; (ii) the aerosol extinction at
801 660 nm extrapolated from CAPS PMex measurements and estimated as the sum of nephelometer
802 scattering and MAAP absorption; (iii) the extinction aerosol Ångstrom exponent; (iv) the aerosol single
803 scattering albedo at 660 nm. Each point in the plot corresponds to 2 min average data. The x-axis
804 indicates the data point sequential number. Experiments with dust samples and kaolinite were
805 realisedoccurred between the 3rd and the 9th of November 2016 and lasted between 1 and 2 hours
806 each. Ambient air data were collected at different steps between the 8th and the 14th November 2016
807 for a total of 7 hours of measurements.

808 **Figure 3.** Ammonium sulfate experiment. Left panel: temporal evolution of the extinction and
809 scattering coefficients measured by the CAPS PMex and the nephelometer at 450 nm (blue scale)
810 and 630 nm (red scale). Each point in the plot corresponds to 2 min average data. Right panel: CAPS
811 PMex versus nephelometer data (10 minutes averages). The $y=x$ line and the results of the linear fit
812 between CAPS and nephelometer data are also shown in the plot.

813 **Figure 4.** CAPS PMex extinction coefficient extrapolated at 660 nm versus nephelometer+MAAP
814 calculated extinction at 660 nm for all experiments (dust, kaolinite, ambient air). Each point in the plot
815 corresponds to 10 min average data. The $y=x$ line and the results of the linear fit between CAPS and
816 nephelometer+MAAP data are also shown in the plot.

817 **Figure 5.** Left panel: estimated f values versus $(1-SSA)$ at 660 nm for dust aerosols. Different
818 symbols are used to distinguish between dust from different sources. The uncertainty of $(1-SSA)$ is
819 the standard deviation over 2-min data, while that of f is calculated with the error propagation formula
820 taking into account the uncertainty of a (± 0.14) and that of $(1-SSA)$. Right panel: f versus SSA at 660
821 nm for all experiments. Different symbols are used to distinguish between different aerosol types. The
822 results of the linear fit between f and $(1-SSA)$ are also reported. Data from Weingartner et al. (2003)
823 (W2003) (extracted from their Figure 4) are also shown in the plot for comparison.

824 **Figure 6.** Top panel: $C_{ref}(W2003)$ (multiple scattering correction obtained by taking into account the
825 shadowing-loading effect correction using the parametrisations by Weingartner et al. (2003)) versus
826 SSA at 450 and 660 nm for mineral dust samples analysed in this study. Different symbols are used
827 to distinguish between dust from different sources. As indicated in Table 2, the difference between
828 C_{ref}^* , $C_{ref}(W2003)$, and $C_{ref}(C2010)$ is very low for mineral dust aerosols. The uncertainty of SSA is the
829 standard deviation over 2-min data, while that of $C_{ref}(W2003)$ is calculated with the error propagation
830 formula taking into account the uncertainty of $\beta_{abs,ref}$ and that of $\beta_{ATT}/R(W2003)$. Bottom panel: C_{ref}
831 versus SSA at 450 and 660 nm for the different aerosol samples analysed in this study. Different
832 symbols are used to distinguish between different aerosol types. Data for both $C_{ref}(W2003)$ and C_{ref}^*
833 (multiple scattering correction obtained not taking into account the shadowing-loading effect correction
834 in aethalometer data) are shown for ambient air aerosols, while for dust and kaolinite, for which the
835 difference between the different formulations is very low, only $C_{ref}(W2003)$ is reported. Data from
836 Weingartner et al. (2003) (W2003) (C_{ref} from their Table 3, and SSA extracted from their Fig. 4) and
837 Collaud Coen et al. (2010) (C2010) (extracted from their Fig. 5) at 660 nm are also shown in the plot
838 for comparison. The results of the linear fits between C_{ref} and SSA for mineral dust and for the entire
839 dataset are also shown in the plot.

840 **Figure 7.** Examples of number size distribution (normalised to the total number concentration) for
841 ammonium sulfate, dust (Niger sample), kaolinite, and ambient air aerosols. Data refer to the mean
842 over each experiment as measured from the SMPS and the OPC. Error bars (standard deviations)
843 have been omitted for the sake of clarity.

844 **Figure 8.** Top panel: $C_{ref}(W2003)$ (multiple scattering correction obtained by taking into account the
845 shadowing-loading effect correction using the parametrisations by Weingartner et al. (2003)) at 450
846 and 660 nm versus the effective diameter coarse $D_{eff,coarse}$ for mineral dust samples analysed in this
847 study. Different symbols are used to distinguish between dust from different sources. The uncertainty
848 of $D_{eff,coarse}$ is the standard deviation over 2-min data, while that of $C_{ref}(W2003)$ is calculated with the
849 error propagation formula taking into account the uncertainty of $\beta_{abs,ref}$ and that of $\beta_{ATT}/R(W2003)$.
850 Bottom panel: C_{ref} at 450 and 660 nm versus the effective diameter coarse $D_{eff,coarse}$ for the different
851 aerosol samples analysed in this study. Different symbols are used to distinguish between different

852 aerosol types. Data for both $C_{\text{ref}}(\text{W2003})$ and C_{ref}^* (multiple scattering correction obtained not taking
853 into account the ~~shadowing-loading~~ effect correction in aethalometer data) are shown for ambient air
854 aerosols, while for dust and kaolinite, for which the difference between the different formulations is
855 very low, only $C_{\text{ref}}(\text{W2003})$ is reported. The results of the linear fits between C_{ref} and $D_{\text{eff,coarse}}$ for
856 mineral dust and for the entire dataset are also shown in the plot.

857

858 **Table 1.** Specifications and references of instruments used during experiments.

Instrument	Property	Operating wavelength (nm)	Time resolution	Flowrate (L min ⁻¹)	Percent uncertainty	Reference
Aethalometer (model AE-31, Magee Sci.)	Spectral absorption coefficient	370, 470, 520, 590, 660, 880, 950	2 min	8	±20% (attenuation coefficient)	Hansen et al. (1984) ; W2003 ; C2010
Multi-Angle Absorption Photometer (MAAP, model 5012, Thermo Sci.)	Single-wavelength absorption coefficient	670	1 min	8	±12%	Petzold and Schönlinner (2004); Petzold et al. (2004 and 2005)
Cavity Attenuated Phase Shift Extinction (CAPS PMex, Aerodyne)	Spectral extinction coefficient	450, 630	1 s	0.85	±5%	Massoli et al. (2010)
Nephelometer (model 3563, TSI Inc.)	Spectral scattering coefficient	450, 550, 700	1 s	18	± 94 0%	Anderson and Ogren Sherman et al. (1998, 2015)
SMPS (DMA model 3080, CPC model 3772, TSI Inc.)	Number size distribution	–	3 min	2	–	De Carlo et al. (2004)
OPC optical particle counter (model 1.109, Grimm Inc.)	Number size distribution	655	6 s	1.2	±15% (diameter optical to geometric conversion); ±10 (concentration)	Heim et al. (2008)

859

860

861 **Table 2.** Summary of experiments and results. The mean and the standard deviation of $D_{\text{eff, fine}}$,
862 $D_{\text{eff, coarse}}$, SSA at 450 and 660 nm, C_{ref}^* , $C_{\text{ref}}(\text{W2003})$, and $C_{\text{ref}}(\text{C2010})$ are reported. As a reminder:
863 C_{ref}^* is the multiple scattering correction obtained not taking into account the ~~shadowing-loading~~ effect
864 correction in aethalometer data; $C_{\text{ref}}(\text{W2003})$ and $C_{\text{ref}}(\text{C2010})$ take the ~~shadowing-loading~~ effect
865 correction into account, by using the parametrisations by Weingartner et al. (2003) (referred as
866 W2003) and Collaud Coen et al. (2010) (referred as C2010), respectively. The maximum of the %
867 difference between C_{ref}^* , $C_{\text{ref}}(\text{W2003})$, and $C_{\text{ref}}(\text{C2010})$ is indicated in the table.

Aerosol ID	Source	$D_{\text{eff, fine}}$ (μm) $D_{\text{eff, coarse}}$ (μm)	SSA 450 nm 660 nm	C_{ref}^* 450 nm 660 nm	$C_{\text{ref}}(\text{W2003})$ 450 nm 660 nm	$C_{\text{ref}}(\text{C2010})$ 450 nm 660 nm	Max % diff C_{ref}^* 450 nm 660 nm
Ammonium sulfate	Sigma-Aldrich 99.999% purity	–	$0.999 \pm (<0.001)$ $0.999 \pm (<0.001)$		–	–	
Niger 1	Sahel (13.52°N, 2.63°E)	0.38 ± 0.01 2.6 ± 0.1	0.93 ± 0.01 0.98 ± 0.01	2.00 ± 0.45 1.87 ± 0.51	2.01 ± 0.45 1.87 ± 0.51	2.02 ± 0.45 1.88 ± 0.51	1.0 % 0.4 %
Niger 2	Sahel (13.52°N, 2.63°E)	0.32 ± 0.02 2.3 ± 0.1	0.92 ± 0.01 0.98 ± 0.01	2.05 ± 0.46 1.89 ± 0.57	2.11 ± 0.47 1.92 ± 0.56	2.10 ± 0.47 1.92 ± 0.57	2.8 % 1.6 %
China	Gobi desert (39.43°N, 105.67°E)	0.44 ± 0.01 3.1 ± 0.2	0.94 ± 0.01 0.98 ± 0.01	2.15 ± 0.48 2.02 ± 0.62	2.16 ± 0.48 2.01 ± 0.62	2.16 ± 0.48 2.02 ± 0.63	0.5 % 0.3 %
Arizona	Sonoran desert (33.15°N, 112.08°W)	0.53 ± 0.02 3.1 ± 0.2	0.96 ± 0.01 0.99 ± 0.01	1.81 ± 0.40 1.76 ± 0.56	1.82 ± 0.41 1.78 ± 0.55	1.82 ± 0.41 1.78 ± 0.57	0.5 % 1.1 %
Tunisia	Sahara desert (33.02°N, 10.67°E)	0.48 ± 0.03 3.2 ± 0.7	0.96 ± 0.01 0.99 ± 0.01	1.97 ± 0.49 1.80 ± 0.42	1.98 ± 0.44 1.80 ± 0.42	1.98 ± 0.44 1.80 ± 0.42	0.5 % 0 %
Australia	Strzelecki desert (31.33°S, 140.33°E)	0.55 ± 0.02 2.4 ± 0.1	0.85 ± 0.01 0.98 ± 0.01	2.52 ± 0.56 2.28 ± 0.74	2.56 ± 0.57 2.26 ± 0.72	2.56 ± 0.57 2.28 ± 0.74	1.6 % 0.9 %
Namibia	Namib desert (19.0°S, 13.0°E)	0.45 ± 0.04 3.6 ± 0.3	0.95 ± 0.01 0.98 ± 0.01	2.02 ± 0.45 1.75 ± 0.57	2.03 ± 0.45 1.76 ± 0.54	2.03 ± 0.45 1.79 ± 0.57	0.5 % 2.2 %
Kaolinite	Source Clay Repository KGa-2	0.39 ± 0.07 2.3 ± 1.6	0.96 ± 0.01 0.97 ± 0.01	2.47 ± 0.55 2.31 ± 0.60	2.51 ± 0.56 2.34 ± 0.60	2.50 ± 0.56 2.33 ± 0.60	1.6 % 1.3 %
Ambient air 1	Suburbs of Paris	0.24 ± 0.08 5.2 ± 0.9	0.79 ± 0.05 0.61 ± 0.08	3.87 ± 0.87 1.97 ± 0.71	4.01 ± 0.90 2.05 ± 0.73	4.03 ± 0.90 2.11 ± 0.76	4.0 % 6.6 %
Ambient air 2	Suburbs of Paris	0.50 ± 0.02 4.5 ± 0.1	0.72 ± 0.04 0.67 ± 0.09	3.22 ± 0.72 1.66 ± 0.44	3.68 ± 0.82 1.94 ± 0.52	3.57 ± 0.80 1.87 ± 0.50	12.5 % 14.4 %
Ambient air 3	Suburbs of Paris	0.46 ± 0.03 6.2 ± 0.7	0.78 ± 0.06 0.54 ± 0.10	3.93 ± 0.88 2.32 ± 0.76	4.35 ± 0.97 2.78 ± 0.89	4.25 ± 0.95 2.68 ± 0.87	21.1 % 16.5 %
Ambient air 4	Suburbs of Paris	0.53 ± 0.05 5.3 ± 1.3	0.63 ± 0.05 0.42 ± 0.08	3.41 ± 0.76 2.25 ± 0.68	3.90 ± 0.87 2.69 ± 0.81	3.79 ± 0.85 2.62 ± 0.79	12.6 % 16.4 %
Ambient air 5	Suburbs of Paris	0.37 ± 0.03 3.4 ± 0.1	0.76 ± 0.08 0.65 ± 0.12	2.72 ± 0.61 2.54 ± 0.82	2.58 ± 0.58 2.51 ± 0.81	2.77 ± 0.62 2.61 ± 0.85	5.4 % 2.7 %
Ambient air 6	Suburbs of Paris	0.37 ± 0.05 4.1 ± 1.0	0.62 ± 0.04 0.46 ± 0.09	2.75 ± 0.50 2.24 ± 0.60	2.78 ± 0.62 2.96 ± 0.79	2.66 ± 0.59 2.79 ± 0.75	19.1 % 24.3 %
Ambient air 7	Suburbs of Paris	0.40 ± 0.01 4.7 ± 0.7	0.87 ± 0.05 0.76 ± 0.08	3.85 ± 0.86 1.86 ± 0.74	4.06 ± 0.91 2.04 ± 0.69	4.01 ± 0.90 2.02 ± 0.80	5.2 % 8.8 %
Ambient air 8	Suburbs of Paris	0.42 ± 0.07 4.3 ± 0.7	0.78 ± 0.06 0.71 ± 0.07	1.91 ± 0.43 2.09 ± 0.61	2.22 ± 0.50 2.53 ± 0.73	2.16 ± 0.48 2.45 ± 0.72	14.0 % 17.4 %

868 **Table 3.** Mean and standard deviation multiple scattering correction $\overline{C_{ref}}$ at 450 and 660 nm for dust,
 869 kaolinite, and ambient air. The $\overline{C_{ref}}$ was calculated as the mean of the C_{ref}^* , $C_{ref}(W2003)$, and
 870 $C_{ref}(C2010)$ obtained at each wavelength for the different aerosol types. As a reminder: C_{ref}^* is the
 871 multiple scattering correction obtained not taking into account the shadowing-loading effect correction
 872 in aethalometer data; $C_{ref}(W2003)$ and $C_{ref}(C2010)$ take the shadowing-loading effect correction into
 873 account, by using the parametrisations by Weingartner et al. (2003) and Collaud Coen et al. (2010),
 874 respectively.

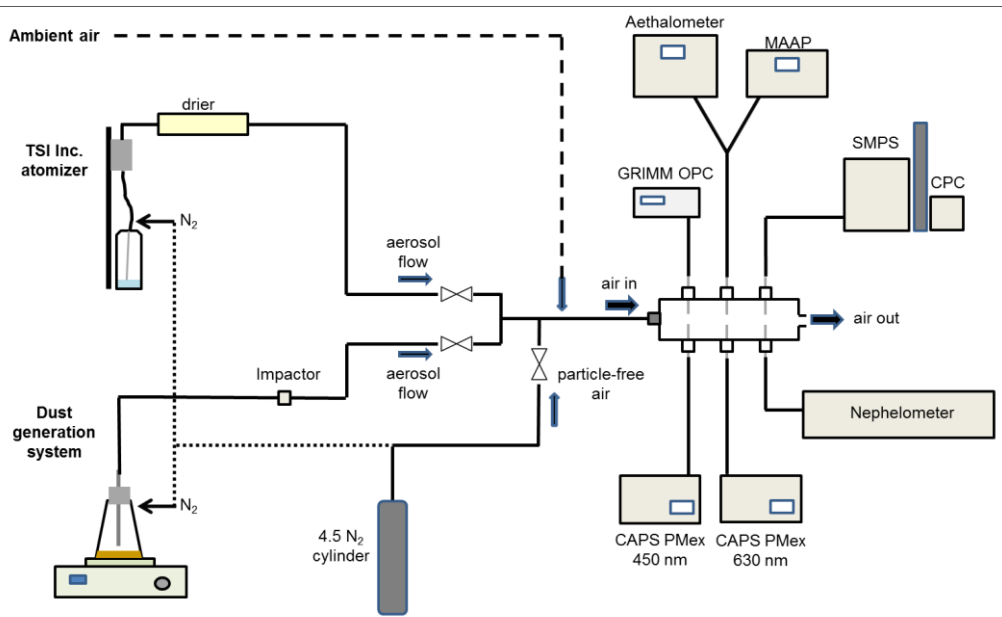
875

	$\overline{C_{ref}}$	
	450 nm	660 nm
Mineral dust	2.09 ± 0.22	1.92 ± 0.17
Kaolinite	2.49 ± 0.02	2.31 2 ± 0.04 2
Ambient air	3.31 ± 0.75	2.32 ± 0.35

876

877

878 **Figure 1.** Experimental setup used for the aethalometer intercomparison experiments.



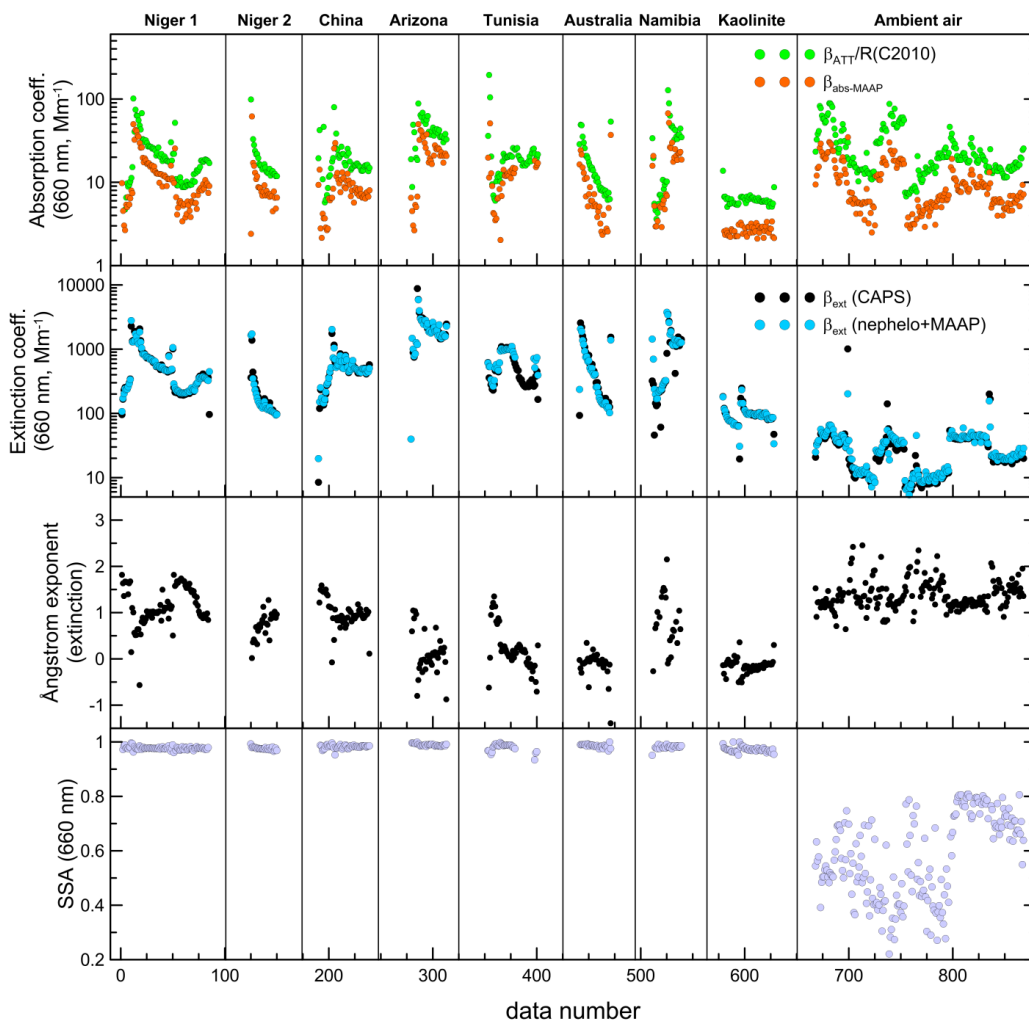
879
880

881

882

883 **Figure 2.** Temporal series of experiments showing the measured optical data at 660 nm. The different
 884 panels show (from the top to the bottom): (i) the **shadowingloading**-corrected aethalometer
 885 attenuation at 660 nm (data corrected with the R formulation by Collaud Coen et al. (2010) (referred
 886 to as R(C2010)) are shown) and the MAAP aerosol absorption coefficient; (ii) the aerosol extinction at
 887 660 nm extrapolated from CAPS PMex measurements and estimated as the sum of nephelometer
 888 scattering and MAAP absorption; (iii) the extinction aerosol Ångstrom exponent; (iv) the aerosol single
 889 scattering albedo at 660 nm. Each point in the plot corresponds to 2 min average data. The x-axis
 890 indicates the data point sequential number. Experiments with dust samples and kaolinite **were**
 891 **realisedoccurred** between the 3rd and the 9th of November 2016 and lasted between 1 and 2 hours
 892 each. Ambient air data were collected at different steps between the 8th and the 14th November 2016
 893 for a total of 7 hours of measurements.

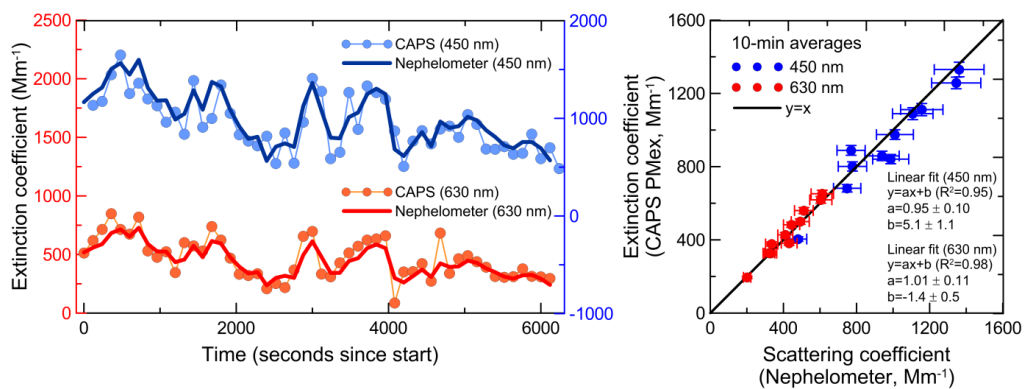
894



895
896

897 **Figure 3.** Ammonium sulfate experiment. Left panel: temporal evolution of the extinction and
 898 scattering coefficients measured by the CAPS PMex and the nephelometer at 450 nm (blue scale)
 899 and 630 nm (red scale). Each point in the plot corresponds to 2 min average data. Right panel: CAPS
 900 PMex versus nephelometer data (10 minutes averages). The $y=x$ line and the results of the linear fit
 901 between CAPS and nephelometer data are also shown in the plot.

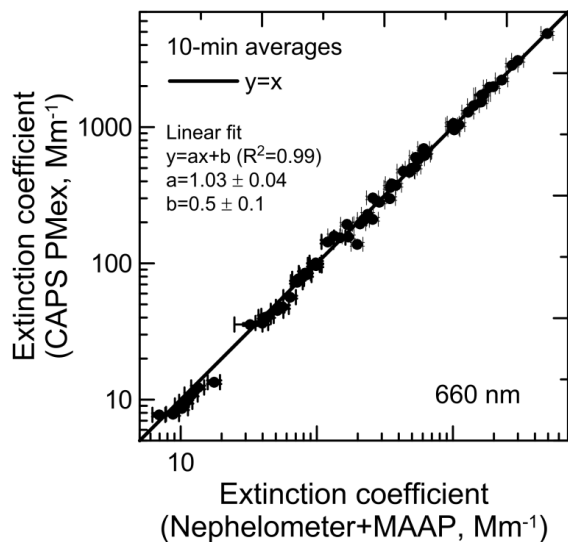
902
 903



904
 905

906 **Figure 4.** CAPS PMex extinction coefficient extrapolated at 660 nm versus nephelometer+MAAP
907 calculated extinction at 660 nm for all experiments (dust, kaolinite, ambient air). Each point in the plot
908 corresponds to 10 min average data. The $y=x$ line and the results of the linear fit between CAPS and
909 nephelometer+MAAP data are also shown in the plot.

910



911

912

913

914

915

916

917

918

919

920

921

922

923

924

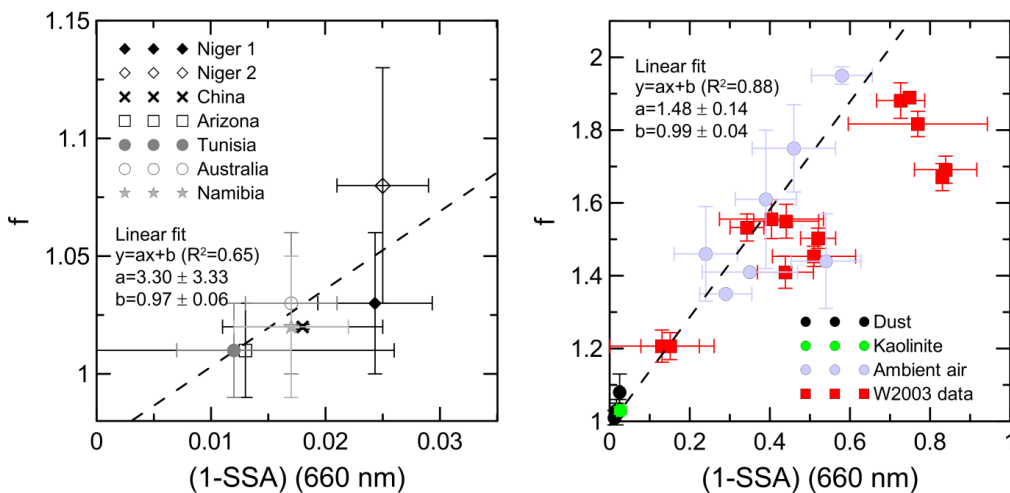
925

926

927 **Figure 5.** Left panel: estimated f values versus $(1-SSA)$ at 660 nm for dust aerosols. Different
928 symbols are used to distinguish between dust from different sources. The uncertainty of $(1-SSA)$ is

929 | the standard deviation over 2-min data, while that of f is calculated with the error propagation formula
 930 | taking into account the uncertainty of a (± 0.14) and that of $(1-SSA)$. Right panel: f versus SSA at 660
 931 | nm for all experiments. Different symbols are used to distinguish between different aerosol types. The
 932 | results of the linear fit between f and $(1-SSA)$ are also reported. Data from Weingartner et al. (2003)
 933 | (W2003) (extracted from their Figure 4) are also shown in the plot for comparison.

934
 935
 936



937
 938

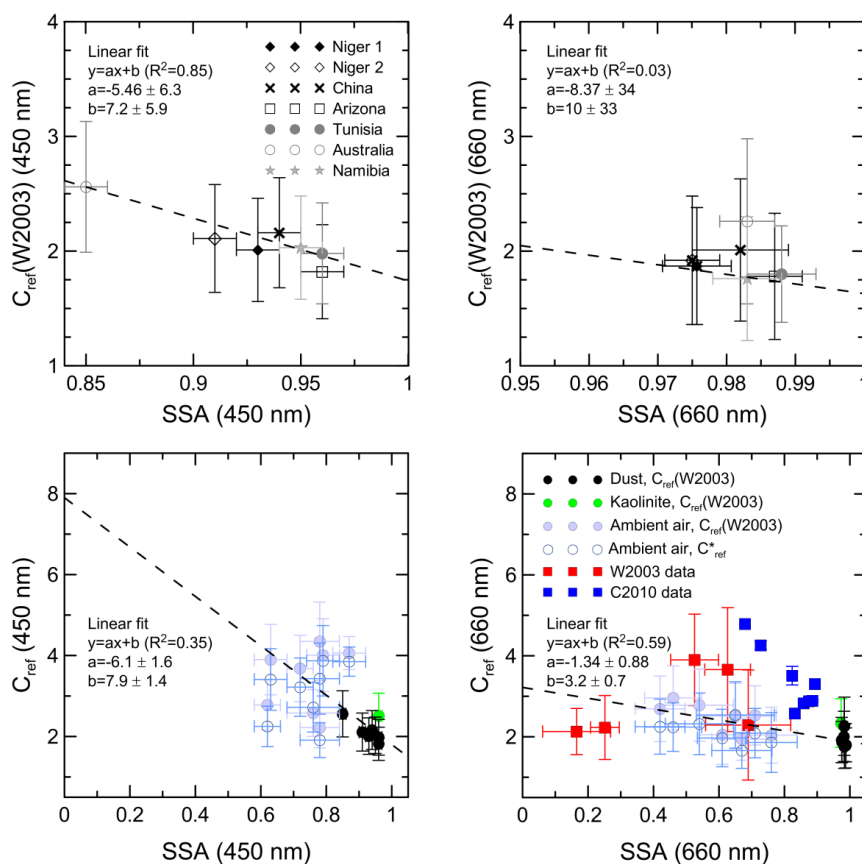
939 **Figure 6.** Top panel: $C_{ref}(W2003)$ (multiple scattering correction obtained by taking into account the
 940 shadowing-loading effect correction using the parametrisations by Weingartner et al. (2003)) versus
 941 SSA at 450 and 660 nm for mineral dust samples analysed in this study. Different symbols are used
 942 to distinguish between dust from different sources. As indicated in Table 2, the difference between
 943 C_{ref}^* , $C_{ref}(W2003)$, and $C_{ref}(C2010)$ is very low for mineral dust aerosols. The uncertainty of SSA is the
 944 standard deviation over 2-min data, while that of $C_{ref}(W2003)$ is calculated with the error propagation
 945 formula taking into account the uncertainty of $\beta_{abs,ref}$ and that of $\beta_{ATT}/R(W2003)$. Bottom panel: C_{ref}
 946 versus SSA at 450 and 660 nm for the different aerosol samples analysed in this study. Different
 947 symbols are used to distinguish between different aerosol types. Data for both $C_{ref}(W2003)$ and C_{ref}^*
 948 (multiple scattering correction obtained not taking into account the shadowing-loading effect correction
 949 in aethalometer data) are shown for ambient air aerosols, while for dust and kaolinite, for which the
 950 difference between the different formulations is very low, only $C_{ref}(W2003)$ is reported. Data from
 951 Weingartner et al. (2003) (W2003) (C_{ref} from their Table 3, and SSA extracted from their Fig. 4) and
 952 Collaud Coen et al. (2010) (C2010) (extracted from their Fig. 5) at 660 nm are also shown in the plot
 953 for comparison. The results of the linear fits between C_{ref} and SSA for mineral dust and for the entire
 954 dataset are also shown in the plot.

Mis en forme : Indice

Mis en forme : Non Exposant/ Indice

955

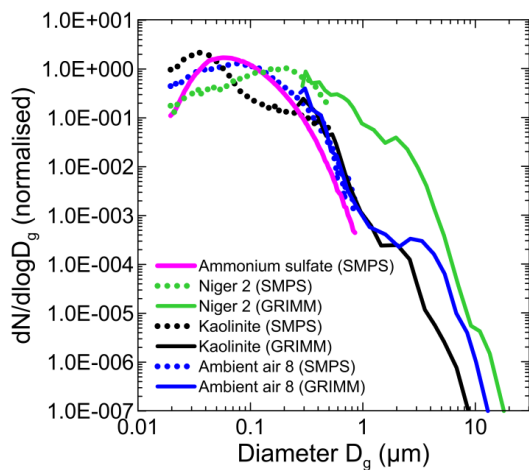
956



957

959 **Figure 7.** Examples of number size distribution (normalised to the total number concentration) for
960 ammonium sulfate, dust (Niger sample), kaolinite, and ambient air aerosols. Data refer to the mean
961 over each experiment as measured from the SMPS and the OPC. Error bars (standard deviations)
962 have been omitted for the sake of clarity.

963



964

965

966 **Figure 8.** Top panel: $C_{ref}(W2003)$ (multiple scattering correction obtained by taking into account the
967 ~~shadowing-loading~~ effect correction using the parametrisations by Weingartner et al. (2003)) at 450
968 and 660 nm versus the effective diameter coarse $D_{eff,coarse}$. for mineral dust samples analysed in this
969 study. Different symbols are used to distinguish between dust from different sources. The uncertainty
970 of $D_{eff,coarse}$ is the standard deviation over 2-min data, while that of $C_{ref}(W2003)$ is calculated with the
971 error propagation formula taking into account the uncertainty of $\beta_{abs,ref}$ and that of $\beta_{ATT/R}(W2003)$.
972 Bottom panel: C_{ref} at 450 and 660 nm versus the effective diameter coarse $D_{eff,coarse}$ for the different
973 aerosol samples analysed in this study. Different symbols are used to distinguish between different
974 aerosol types. Data for both $C_{ref}(W2003)$ and C_{ref}^* (multiple scattering correction obtained not taking
975 into account the ~~shadowing-loading~~ effect correction in aethalometer data) are shown for ambient air
976 aerosols, while for dust and kaolinite, for which the difference between the different formulations is
977 very low, only $C_{ref}(W2003)$ is reported. The results of the linear fits between C_{ref} and $D_{eff,coarse}$ for
978 mineral dust and for the entire dataset are also shown in the plot.

979

